



RESEARCH ARTICLE

10.1002/2016JD025596

Key Points:

- Coupled model rainfall climatologies differ by up to a factor of 5 over the Congo
- Moisture flux convergence is strongly related to rainfall at particular levels in the atmosphere in different seasons
- Measurements of moisture flux at the basin boundaries could constrain spectrum of model rainfall

Supporting Information:

- Supporting Information S1

Correspondence to:

A. Creese,
amy.creese@ouce.ox.ac.uk

Citation:

Creese, A., and R. Washington (2016), Using qflux to constrain modeled Congo Basin rainfall in the CMIP5 ensemble, *J. Geophys. Res. Atmos.*, 121, 13,415–13,442, doi:10.1002/2016JD025596.

Received 29 JUN 2016

Accepted 7 NOV 2016

Accepted article online 14 NOV 2016

Published online 26 NOV 2016

Using qflux to constrain modeled Congo Basin rainfall in the CMIP5 ensemble

A. Creese¹ and R. Washington¹
¹School of Geography and the Environment, University of Oxford, Oxford, UK

Abstract Coupled models are the tools by which we diagnose and project future climate, yet in certain regions they are critically underevaluated. The Congo Basin is one such region which has received limited scientific attention, due to the severe scarcity of observational data. There is a large difference in the climatology of rainfall in global coupled climate models over the basin. This study attempts to address this research gap by evaluating modeled rainfall magnitude and distribution amongst global coupled models in the Coupled Model Intercomparison Project 5 (CMIP5) ensemble. Mean monthly rainfall between models varies by up to a factor of 5 in some months, and models disagree on the location of maximum rainfall. The ensemble mean, which is usually considered a “best estimate” of coupled model output, does not agree with any single model, and as such is unlikely to present a possible rainfall state. Moisture flux (qflux) convergence (which is assumed to be better constrained than parameterized rainfall) is found to have a strong relationship with rainfall; strongest correlations occur at 700 hPa in March–May ($r = 0.70$) and 850 hPa in June–August, September–November, and December–February ($r = 0.66$, $r = 0.71$, and $r = 0.81$). In the absence of observations, this relationship could be used to constrain the wide spectrum of modeled rainfall and give a better understanding of Congo rainfall climatology. Analysis of moisture transport pathways indicates that modeled rainfall is sensitive to the amount of moisture entering the basin. A targeted observation campaign at key Congo Basin boundaries could therefore help to constrain model rainfall.

1. Introduction

Global coupled climate models (GCMs) are crucial to developing climate projections, yet in certain regions they are critically understudied and underevaluated. Africa is one such region which has historically received little climatic attention, a problem which has begun to be addressed in earnest through the creation of several targeted research projects, for example, the Natural Environment Research Council (NERC)/Department for International Development (DFID)-funded Future Climate for Africa. However, glaring omissions remain in the map of African climate research; in particular, the Congo Basin, which has been subject to less targeted research than any other African region [Washington *et al.*, 2006]. This is despite the crucial role the Congo plays in both the regional and global climate systems.

The importance of the Congo is based upon three key considerations. First, it is one of three global convective hot spots [Webster, 1983], experiencing the highest lightning strike frequency of anywhere on the planet [Jackson *et al.*, 2009] and dominating global rainfall totals in the transition seasons [Xie *et al.*, 2003]. Second, the region's forests are a globally significant carbon sink and, thus, a crucial element of the climate system via the carbon cycle [Williams *et al.*, 2007]. It is estimated that 60–70 Pg of carbon is stored in above-ground vegetation in Africa, second only to the amount stored in Amazonia [Baccini *et al.*, 2012]. During the dry seasons, Congo forests are particularly vulnerable due to their proximity to the rainfall threshold below which rainforest ecosystems transition to savannah [Malhi *et al.*, 2013]. Projections indicate that pronounced warming over Africa could result in drier and more extended dry seasons, further increasing the region's vulnerability [James and Washington, 2013]. Third, the region's population relies heavily on rain-fed agriculture and has already experienced severe land degradation due to drought in recent years [Samba and Nganga, 2012]. Climate prediction is therefore crucial to these populations.

The most significant limitation to climatic research in the Congo Basin is the dearth of observational data, primarily the result of the extreme ratio of size to access of the region, exacerbated by political instability in recent decades. Historical data sets have been compiled for the region [e.g., Aguilar *et al.*, 2009; Nicholson *et al.*, 2012], but the number of maintained rain gauges has been in rapid decline since the 1980s (Figure 1) [Harris *et al.*, 2014]. Only three meteorological stations in the Democratic Republic of the Congo

©2016. The Authors.

This is an open access article under the terms of the Creative Commons Attribution License, which permits use, distribution and reproduction in any medium, provided the original work is properly cited.

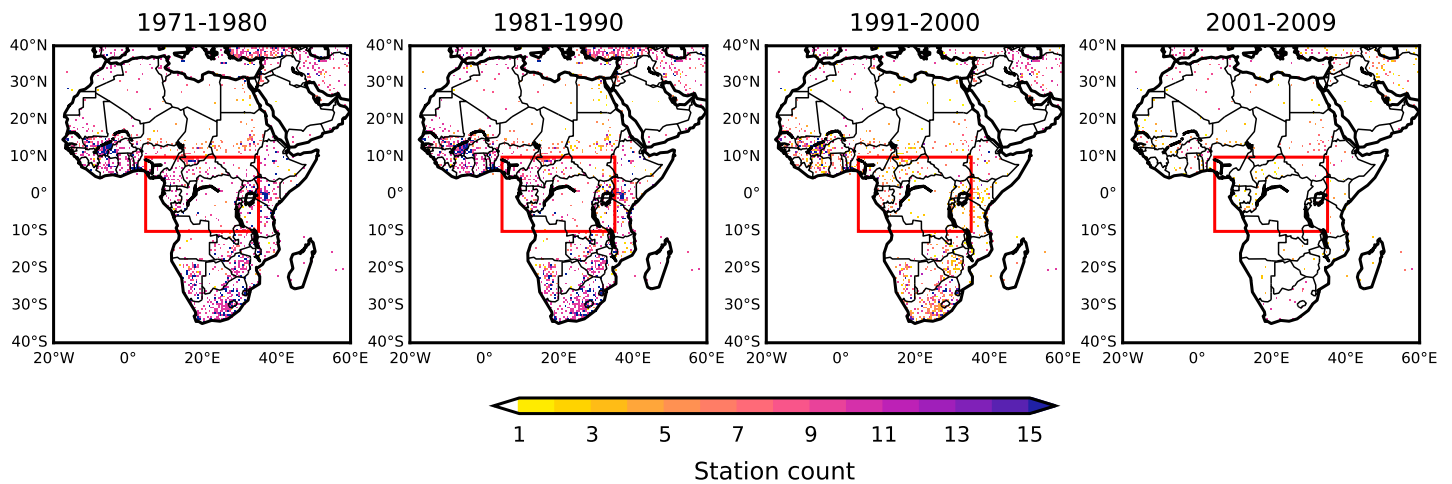


Figure 1. Mean number of stations contributing to the CRU 3.10 gridded precipitation data set (0.5° horizontal grid spacing). Red box indicates study domain for this research (5°E to 35°E, 10°N to 10°S).

reported to the Global Telecommunication System in 2013; this compares to over 3000 stations which report to the Met Office in the UK alone (an area 40 times smaller). Nevertheless, the Congo's significance is increasingly being recognized in scientific literature, not least because anthropogenic-induced climatic changes have been brought to the forefront of African environmental policy [James and Washington, 2013]. Several recent studies have utilized satellite, gauge, and reanalyses data in equatorial Africa to identify controls on both seasonal and interannual rainfall variability, with particular reference to the characteristics of: the African easterly jet [Nicholson and Grist, 2003; Dezfuli and Nicholson, 2011], low-level westerlies [Dezfuli and Nicholson, 2011; Pokam et al., 2014], mesoscale convective systems [Jackson et al., 2009], sea surface temperature (SST) teleconnections [Nicholson and Dezfuli, 2013; Hirst and Hastenrath, 1983; Hansingo and Reason, 2009], and zonal overturning circulations across the region [Cook and Vizi, 2015].

1.1. Congo Climate Regime

The key features of the Congo Basin climate regime are shown in Figure 2. The region (here defined as 5°E to 35°E, 10°N to 10°S, shown by the red box in Figure 1) is strongly influenced by the latitudinal march of tropical convection, which lags solar heating by roughly a month. Rainfall oscillates meridionally, crossing the equator twice a year during the transition seasons of March to May (MAM) and September to November (SON), with dry seasons in June to August (JJA) and December to January (DJF). MAM events appear to be heavier and more prolonged, whereas SON rains are relatively short and less intense [Sandjon et al., 2012]; Jackson et al.'s [2009] study would suggest that this is due to enhanced mesoscale convective system activity. The zone of maximum rainfall occurs broadly over the western central African region, covering almost the entirety of the Congo forest [Pokam et al., 2012] and coinciding with a locus of intensive convective activity [Sandjon et al., 2012].

One of the key drivers of Congo rainfall variability is the availability, transport, and accumulation of moisture in the atmosphere. Pokam et al. [2012] suggest that there are two maxima of moisture convergence: the first during the MAM wet season, resulting from moisture flux near 700 hPa and embedded in the northerly component of the African easterly jet (AEJ-N), and the second during SON at lower levels (850–1000 hPa), dominated by advection from the Atlantic. Such results, in addition to those of Washington et al. [2013], indicate that assessment of moisture transport into the region could help constrain coupled model outputs. Moisture convergence has been utilized similarly in the Amazon by Yin et al. [2013]; satellite and ground-based measurements were used to determine the cause of rainfall underestimation in Amazonia in Coupled Model Intercomparison Project 3 (CMIP3) and CMIP5 models. They conclude that models featuring the most realistic moisture convergence and evapotranspiration values also feature the most realistic rainfall

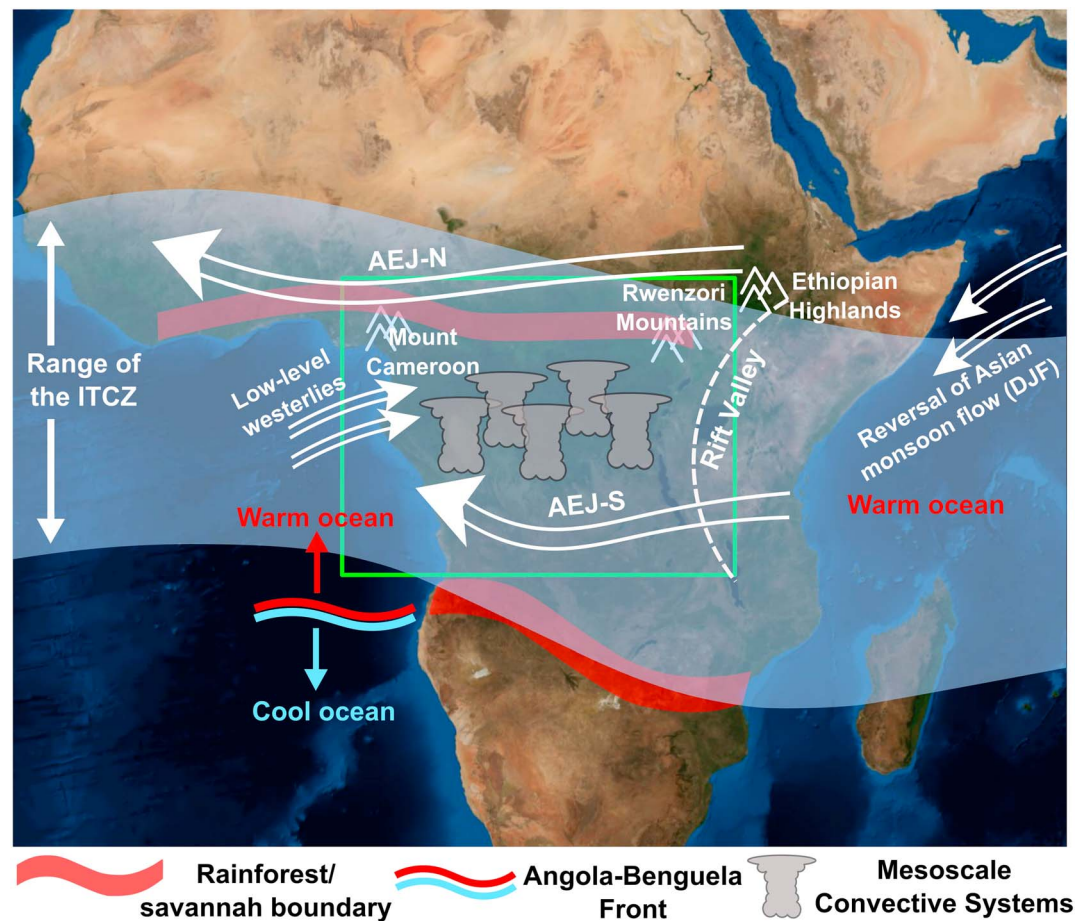


Figure 2. Schematic showing key features of the Congo Basin climate. Locations are approximate. The study area is shown by the green box. AEJ-N = African easterly jet, north and AEJ-S = African easterly jet, south. Background image: NASA Visible Earth.

magnitudes, particularly in the dry seasons. Models which overestimate moisture divergence feature the strongest rainfall underestimations, pointing to a strong relationship between moisture flux convergence and modeled rainfall.

1.2. Coupled Models

Coupled models are increasingly being used to diagnose present and future changes in African climate. They have been utilized extensively in the Sahel, the most studied region in Africa, due to the multi-decadal drought in the latter half of the twentieth century [Washington *et al.*, 2013], and in some instances have provided a good simulation of Sahelian climate [e.g., Lau *et al.*, 2006]. Multimodel ensembles (MMEs) have also been utilized in West and Southern Africa, with some success [Cook and Vizi, 2006; Lau *et al.*, 2006; Kay and Washington, 2008]. Validation of model hindcasts with reference to observations is a frequently used method [Flato *et al.*, 2013]. Rowell *et al.* [2015] ranked 39 coupled models according to their ability to simulate historical observations in a range of metrics over the Sahel and Greater Horn of Africa; and the process-based assessments of Dieppois *et al.* [2015] and James *et al.* [2015] (of Southern Africa and the Sahel, respectively) rely on the ability of models to reproduce observed patterns of variability. Such methods have also been used over central Africa; Aloysius *et al.* [2016] identified a subset of models based on historical performance metrics which could be used to produce projections with smaller uncertainties, and Haensler *et al.* [2013] compared projections from CMIP3, CMIP5, and Coordinated Regional Climate Downscaling Experiment (CORDEX) to

reanalysis data, concluding that most models have “substantial skill in representing observed conditions” (p.16).

However, despite this progress, there remain substantial inconsistencies between models themselves, as well as between models and observations [Christensen *et al.*, 2013]. These differences are starkest in the Congo Basin, where the lack of observational data poses a challenge to traditional model evaluation techniques. Reanalyses data are commonly used in place of “pure” observations, as they have continuous spatial and temporal coverage. However, for a large region with little or no initialization, the reanalysis process will be steered significantly more by the model; thus, it cannot be regarded as indicative of observations. Indeed, initial analysis of model, reanalyses, and satellite/gauge data suggest that at present there is little agreement between individual datasets as to the quantity and distribution of rainfall across the basin [Washington *et al.*, 2013], even amongst reanalyses data sets themselves. In addition, satellite and gauge estimates have been found to differ by a factor of 2–3 in this region [McCollum *et al.*, 2000; Nicholson *et al.*, 2003].

1.3. Aims

In light of these challenges, this study aims to understand relative differences between models, rather than comparing hindcast output to observations. To do this, we examine the extent to which large-scale patterns of moisture flux and convergence can explain differences in rainfall amongst models. This broad-scale approach is not only necessary due to the coarse resolution of coupled models but also may contribute to a refined understanding of the wide spectrum of rainfall regimes present across the model suite. This is a first step in understanding the extent to which global models are capable of producing usable outputs for this region. We also aim to understand the relationship between rainfall and moisture transported into the basin; if this can be achieved, addressing the data gap for the Congo becomes a more feasible task.

The following section describes the model, reanalysis, satellite, and gauge data used throughout the paper. Section 3 outlines the simulated rainfall climatology in all seasons across models, and an assessment of the relationship between rainfall and moisture flux convergence follows in sections 4 and 5. Finally, the likely origins of water vapor advected into the basin, and its relationship with rainfall between models, are assessed in section 6. Sections 7 and 8 discuss the results and conclude.

2. Data

The focus of this study is the model output from the Coupled Model Intercomparison Project 5 (CMIP5), the most recent large-scale suite of model products from the international community [Taylor *et al.*, 2012]. The experimental design of CMIP5 allows for the creation of multimodel ensembles, which have been shown to produce some of the most accurate simulations of the present climate [Palmer *et al.*, 2005; Reichler and Kim, 2008], including in studies of tropical rainfall [Gulizia and Camilloni, 2014]. This study focuses on the historical experiment, and one model run is analyzed for each model.

Monthly and seasonal means (MAM, JJA, SON, and DJF) of u and v winds, rainfall, specific humidity, and sea surface temperature (SST) from 17 models (Table 1; chosen to include dissimilar models) for the period 1971–2000 inclusive were computed from CMIP5 data which had been interpolated to a common grid spacing of $1.875^\circ \times 1.875^\circ$. Tests of the metrics used in this paper at model native resolution indicate that interpolation does not substantially change the results.

Reanalysis and observational data are also included as a point of comparison (Table 2). Reanalyses data have been interpolated to the same resolution as models. Native resolution is retained for the observational data sets. Observed SST data are taken from the HadISST.2 data set [Titchner and Rayner, 2014].

3. Rainfall Climatology

3.1. Annual Cycle of Rainfall

All observational and reanalyses data sets feature the expected semiannual cycle of rainfall, with peaks in transition seasons MAM and SON (Figure 3). CRU, GPCC, CMAP, NCEP, GPCP, and TRMM feature peak MAM rainfall in April; ERAI is the only data set to experience peak rainfall in March.

Table 1. CMIP5 Models Used in This Study

Model	Institute	Native Horizontal Resolution	Reference
ACCESS1-3	Commonwealth Scientific and Industrial Research Organization and Bureau of Meteorology Australia (CSIRO-BOM)	1.25° × 1.875°	Collier and Uhe [2012]
BNU-ESM	College of Global Change and Earth System Science, Beijing Normal University	2.81° × 2.79°	Ji et al. [2014]
CanESM2	Canadian Centre for Climate Modelling and Analysis (CCCma)	2.81° × 2.79°	Yang and Saenko [2012]
CESM1-CAM5	National Centre for Atmospheric Research (NCAR)	1.25° × 1.0°	Neale et al. [2012]
CMCC-CMS	Centro Euro-Mediterraneo per I Cambiamenti Climatici (CMCC)	1.87° × 1.87°	Scoccimarro et al. [2011]
CNRM-CM5-2	Centre National de Recherches Météorologiques / Centre Européen de Recherche et Formation Avancée en Calcul Scientifique (CNRM-CERFACS)	1.4° × 1.4°	Voltaire et al. [2011]
CSIRO-Mk3-6-0	Commonwealth Scientific and Industrial Research Organization in collaboration with Queensland Climate Change Centre of Excellence (CSIRO-QCCCE)	1.9° × 1.9°	Jeffrey et al. [2013]
GFDL-CM3	NOAA Geophysical Fluid Dynamics Laboratory (NOAA GFDL)	2.5° × 2.0°	Donner et al. [2011]
GFDL-ESM2G	NOAA Geophysical Fluid Dynamics Laboratory (NOAA GFDL)	2.5° × 2.0°	Dunne et al. [2013]
GISS-E2-H-CC	NASA Goddard Institute for Space Studies (GISS)	2.5° × 2°	Schmidt et al. [2013]
HadGEM2-ES	Met Office Hadley Centre (MOHC)	1.9° × 1.3°	Jones et al. [2011]
IPSL-CM5A-MR	Institut Pierre-Simon Laplace (IPSL)	2.50° × 1.26°	Dufresne et al. [2013]
MIROC5	Atmosphere and Ocean Research Institute (University of Tokyo), National Institute for Environmental Studies, and Japan Agency for Marine-Earth Science and Technology (MIROC)	1.40° × 1.40°	Watanabe et al. [2010]
MIROC-ESM	Atmosphere and Ocean Research Institute (University of Tokyo), National Institute for Environmental Studies, and Japan Agency for Marine-Earth Science and Technology (MIROC)	2.81° × 2.79°	Watanabe et al. [2011]
MPI-ESM-LR	Max-Planck-Institut für Meteorologie (MPI-M)	1.9° × 1.9°	Marsland et al. [2003]
MRI-ESM1	Meteorological Research Institute (MRI)	1.125° × 1.125°	Yukimoto et al. [2011]
NorESM1-M	Norwegian Climate Centre (NCC)	2.5° × 1.9°	Bentsen et al. [2013]

All models are able to broadly reproduce the annual distribution of rainfall, with peaks at MAM and SON (Figure 3, 30-year mean). The majority of models (13/17) exhibit peak MAM rainfall in April; peak SON rainfall is in October (12 models) or November (5 models). All models agree on the month of boreal summer rainfall minimum (July), which is 1–2 months later than all observational data sets (except ERAI). Models place the DJF minimum in January (13/17) or February (4/17). The wettest monthly value features in October (MIROC5, 7.8 mm d⁻¹), with a second rainfall maximum in November (NorESM1-M, 7.8 mm d⁻¹). MAM peak rainfall is seen in April (MIROC5, 7.6 mm d⁻¹). The driest monthly value is in January (CSIRO-Mk3-6-0, 0.9 mm d⁻¹). July features the lowest JJA value (MRI-ESM1, 2.3 mm d⁻¹).

Table 2. Definition and Characteristics of Reanalysis and Satellite/Gauge Data Sets Used in This Study

Data Set	Full Name and Institute	Native Horizontal Resolution	Dates Used	Reference
ERA-Interim	European Centre for Medium Range Weather Forecasts	0.7° × 0.7°	1981–2010	Dee et al. [2011]
NCEP/NCAR	National Centers for Environmental Prediction (NCEP) and the National Center for Atmospheric Research (NCAR)	2.5° × 2.5°	1971–2000	Kalnay et al. [1996]
CRU	Climate Research Unit, University of East Anglia (v3.10)	0.5° × 0.5°	1971–2000	Harris et al. [2014]
GPCC	Global Precipitation Climatology Centre, Deutscher Wetterdienst, World Meteorological Organization	0.5° × 0.5°	1971–2000	Schneider et al. [2015]
CMAP	Climate Prediction Centre Merged Analysis of Precipitation, NOAA NCEP	2.5° × 2.5°	1971–2000	Xie and Arkin [1997]
GPCP	Global Precipitation Climatology Project, World Climate Research Programme (WCRP)	2.5° × 2.5°	1981–2010	Adler et al. [2003]
TAMSAT	Tropical Applications of Meteorology using Satellite data and ground-based observations, University of Reading	0.0375° × 0.0375°	1983–2011	Maidment et al. [2014]
TRMM	Tropical Rainfall Measuring Mission, NASA Goddard Space Flight Center, Japanese Aerospace Exploration Agency	0.25° × 0.25°	1998–2014	Huffman et al. [2007]

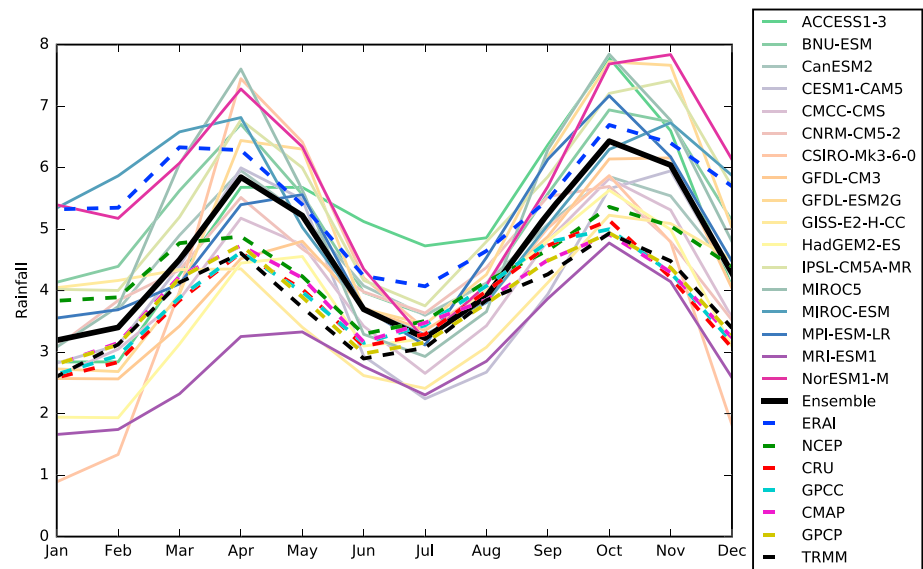


Figure 3. The 30 year mean rainfall (mm d^{-1}) for individual CMIP5 models, reanalysis, and satellite data for 1971–2000.

Despite all models and data sets reproducing the semiannual cycle of rainfall, there are large differences amongst annual cycles. The largest spread of absolute values occurs in November, where the difference between the wettest and driest data set is 6.0 mm d^{-1} (standard deviation = 1.36 mm d^{-1}); this equates to 180 mm difference over the month. The smallest absolute range is seen in August (2.2 mm d^{-1}), and the smallest standard deviation is in July (0.6 mm d^{-1}). In several cases, the dry season minimum of some models is wetter than wet season values for other models, and vice versa. For example, the JJA minimum in ACCESS1-3 (July, 4.7 mm d^{-1}) is wetter than the MAM maximum in GISS-E2-H-CC (April, 4.4 mm d^{-1}); NorESM1-M's DJF minimum (January, 5.4 mm d^{-1}) is 0.6 mm d^{-1} wetter than GFDL-CM3's MAM maximum (May, 4.8 mm d^{-1}).

3.2. Rainfall Distribution

3.2.1. Wet Seasons

To compare the spatial distribution of rainfall across data sets, long-term (30 year) means are plotted for central Africa across all seasons. Models have been ordered dry to wet (reading left to right across Figure 4) based on mean rainfall magnitudes for that season. As expected from the wide variation in rainfall magnitudes, there are large differences in rainfall distribution between models. In MAM (Figure 4a), drier models (e.g., MRI-ESM1, HadGEM2-ES, and GISS-E2-H-CC) have much less rainfall over land than wetter models in the ensemble (e.g., NorESM1-M and MIROC5). Rainfall is focused on the Atlantic coast and over the Gulf of Guinea, leading to a western position of the rainfall maxima. In contrast, wetter models have much more rainfall in the east of the basin and relatively less coastal rainfall. To highlight these differences, composites of the five wettest and five driest models are shown in Figure 5a, as well as difference plots. To indicate where there is strong agreement that the wet and dry composites differ, stipples occur for the following conditions: (1) where all wet model values are greater than the mean of dry model values and (2) where all wet model values are greater than the maximum value of dry models. Similarly, crosses indicate (1) where all dry model values are less than the mean of wet model values and (2) where all dry model values are less than the minimum value of dry models.

Figure 5a shows that the five wettest models produce an eastern maximum when composited, whereas the five driest show a western maximum (though smaller in magnitude). Wet models are on average $2\text{--}3 \text{ mm d}^{-1}$ wetter over the whole of the Congo Basin, with significant differences particularly in the center and east of the domain (Figure 5a). Dry models are significantly drier over a large portion of the domain based on both agreement metrics, and the area of agreement extends farther north than for wet agreement. This suggests that dry models are more consistently dry than wet models in the wider region. Models in the middle of the distribution do not fall into such obvious distributions; some have more easterly rainfall

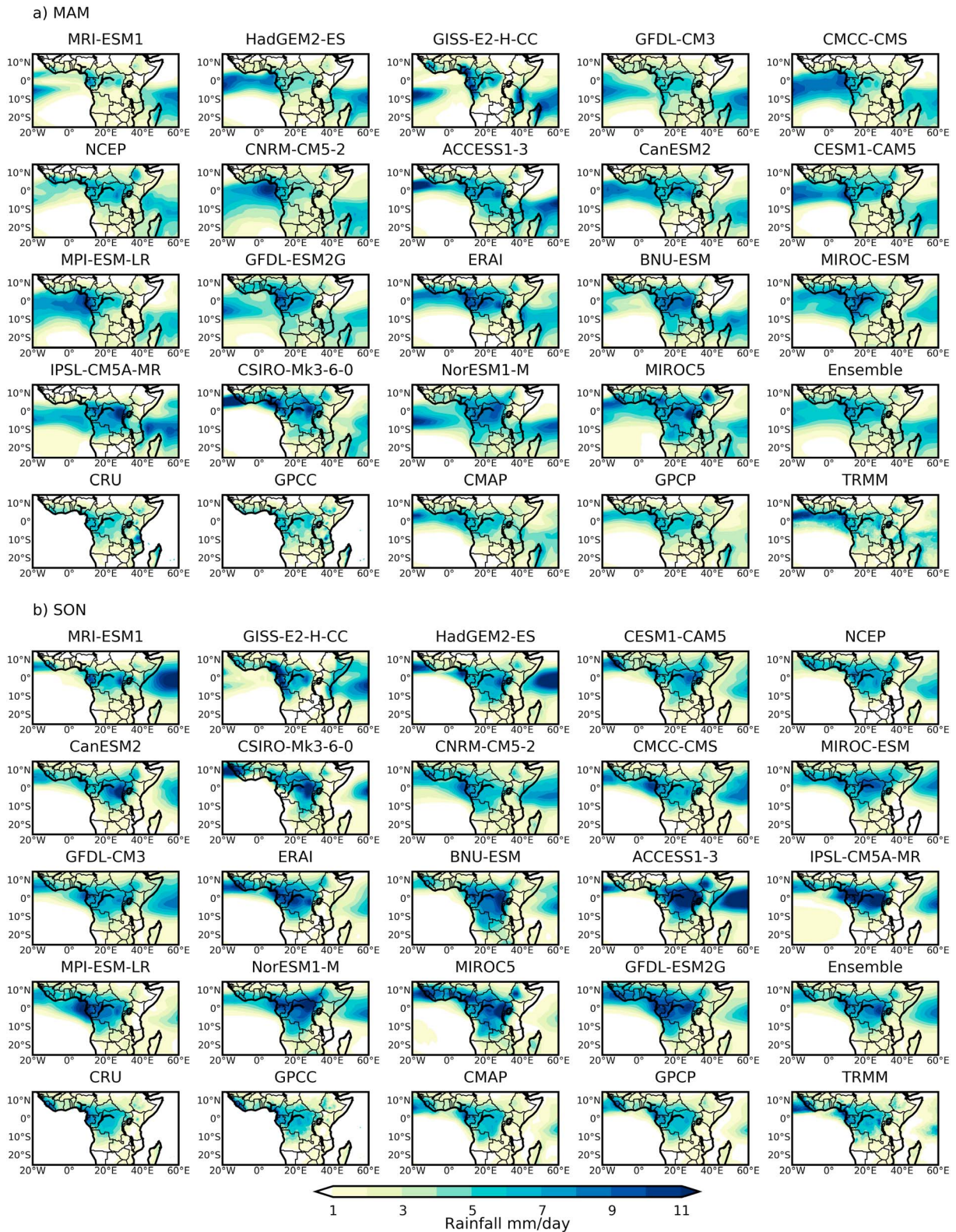


Figure 4. Long-term mean (1971–2000) rainfall (mm d^{-1}) for (a) MAM and (b) SON for 17 CMIP5 models, the ensemble mean, reanalysis, gauge, and satellite data sets. Models are ordered from dry to wet based on mean rainfall across the basin.

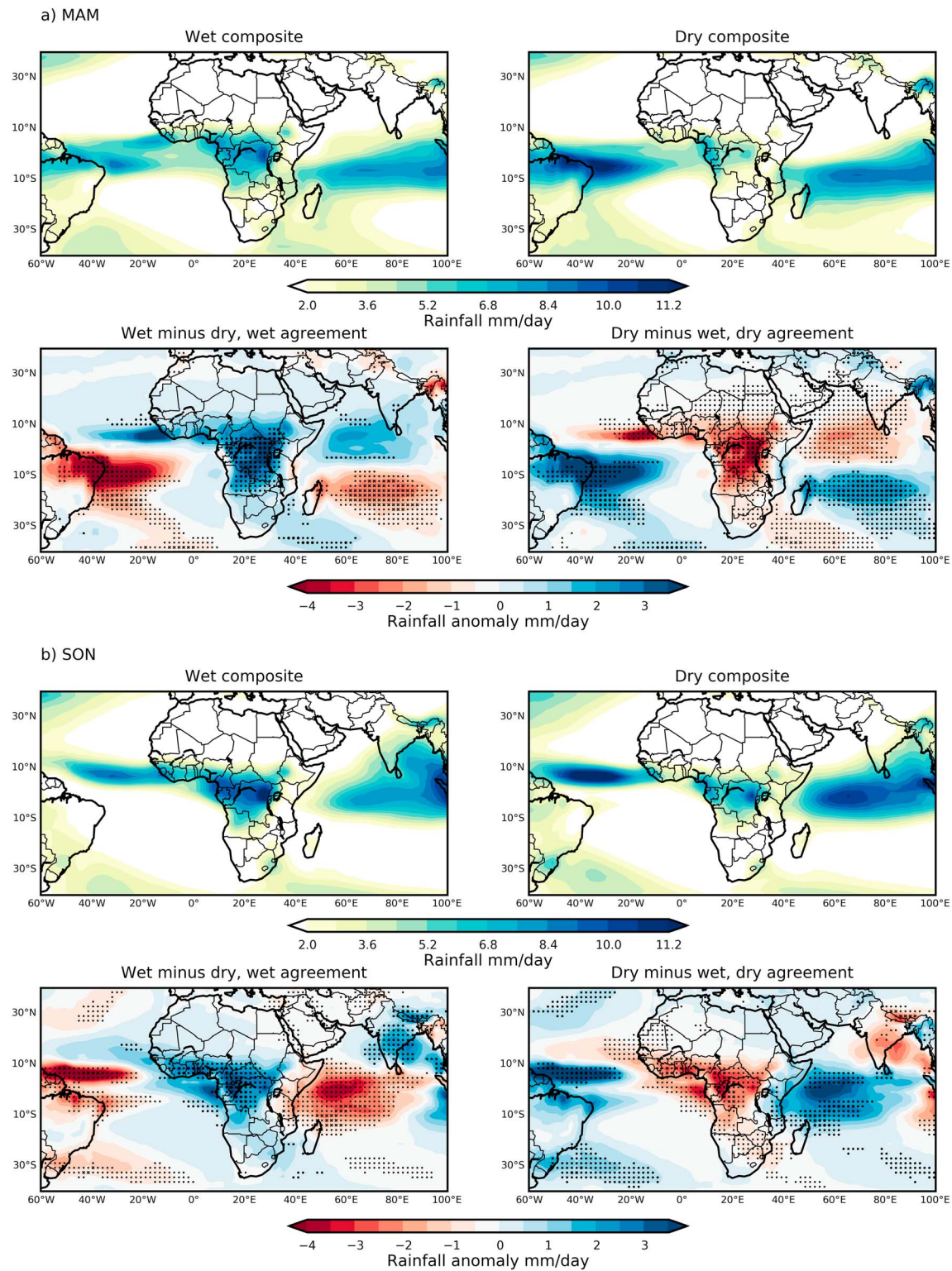


Figure 5. For long-term mean (30 year) rainfall (mm d^{-1}) (a) MAM and (b) SON: composite of five wettest models in Figure 4 (top left); composite of five driest models in Figure 4 (top right); wet composite minus dry composite with stipples for agreement, (bottom left); dry composite minus wet composite, with stipples for agreement (bottom right). Large circles (crosses) indicate that all wet (dry) models are wetter (drier) than the maximum (minimum) of the dry (wet) models at that grid point. Small circles (crosses) indicate that all wet (dry) models are wetter (drier) than the mean of the dry (wet) models at that grid point.

(BNU-ESM), some more westerly (MIROC-ESM), and some have several, spatially disconnected areas of high rainfall (CSIRO-Mk3-6-0). Reflecting these stark differences amongst models, the ensemble mean features a reasonably uniform distribution across the domain. In addition to differences over land, there are also significant differences in rainfall over the oceans. Wet models are wetter in the northwest Indian Ocean but drier over the southwest Indian Ocean and the southwest Atlantic. This points to a possible influence of model sea surface temperatures (SSTs) on rainfall in this region; this is discussed further in section 6.

The second wet season SON also features obvious differences amongst models (Figure 4b). Dry models tend to feature more of their rainfall along the Atlantic coast, as in MAM, although there is less rain over the ocean than in MAM. The majority of models also feature an area of rainfall maxima in the east; this intensifies along the spectrum of dry to wet models. The wettest models have high rainfall across the whole of the basin. Figure 5b shows that the distribution in the composites is quite similar, with higher intensity rainfall in the wet models. Dry models tend to have two relatively weaker maxima, whereas wet models have one strong maximum in the east that extends zonally across the basin. The land/ocean precipitation difference is starker than in MAM; wet models (over land) are significantly drier in the western central Indian Ocean than drier models. Again, this indicates that local SSTs may be one factor influencing model rainfall differences.

3.2.2. Dry Seasons

The magnitude and distribution of dry season Congo rainfall is important to global and regional processes [Malhi *et al.*, 2013], in particular the climatological regulation of the rainforest. As expected, in JJA the zone of tropical convection shifts northward from its position in MAM; this is evident in all models (Figure 6a). Distributional differences are not as obvious as in the wet seasons; all models show a clear western rainfall maximum in the northwest corner of the domain. Several also feature a second rainfall maximum in the northeast corner of the basin; this is stronger in the wettest models and less evident or nonexistent in the drier models (e.g., GISS-E2-H-CC and CESM1-CAM5). Differences between the wet and dry composites are significant over this zonal region (Figure 7a). Differences over the adjacent oceans are not as significant as in the wet seasons.

In DJF, the band of tropical convection has shifted southward, and most models feature the majority of their rainfall over land and in the central Indian Ocean (Figure 6b). In the wettest models (MIROC-ESM and NorESM1-M) the area of rainfall extends northward beyond the equator; in the dry models, it is limited to the region below 5°S, reducing the amount of rainfall in the defined Congo Basin domain. There is not a distinct east/west distinction between wet and dry models (Figure 6b); however, some have a more westerly distribution (e.g., CNRM-CM5-2 and ERAI). The difference in rainfall magnitude between wet and dry models is the largest for any season, exceeding 3 mm d⁻¹ across the majority of the domain. As in MAM, dry models are more consistently dry across the wider African region, as noted by the wider expanse of stipples (Figure 7b), and there is a dipole in rainfall over the Indian Ocean: wet models are wetter in the northwest Indian Ocean and drier in the southwest Indian Ocean. As in all seasons, the ensemble mean does not agree with any one model.

3.2.3. Seasonal Comparisons

Figures 4–7 indicate some distinct patterns in the organization of rainfall amongst models. Figure 8 quantifies the similarities between models across seasons, showing that models tend to be wet or dry across all seasons ($r=0.70$). There is also a significant ($p < 0.05$) positive relationship between rainfall in MAM and SON ($r=0.74$), MAM and JJA ($r=0.49$), MAM and DJF ($r=0.56$), SON and JJA ($r=0.63$), and SON and DJF (0.50). The only seasons where the relationship is not significant are between JJA and DJF; this is perhaps expected as rainfall in the northernmost and southernmost part of the domain is influenced by different large- and regional-scale systems. Nevertheless, when taken as a whole, it is clear that models have a tendency to be generally wetter or drier, regardless of season. This is reinforced by Figure 9, which shows the average rank (dry to wet) for each model and the range in ranks that model populates for the wet seasons (Figure 8a), the dry seasons (Figure 8b), and all seasons (Figure 8c). In wet seasons, the three driest models on average (indicated by the order of the models) rank consistently in that position in both MAM and SON. Similarly, three of the four wettest models are consistently wet. The story is somewhat similar in the dry seasons. There is greater spread in ranks across all four seasons, but at the extreme ends the error bars remain smaller. Of particular note is MRI-ESM1, which is consistently ranked the driest or second driest in all seasons.

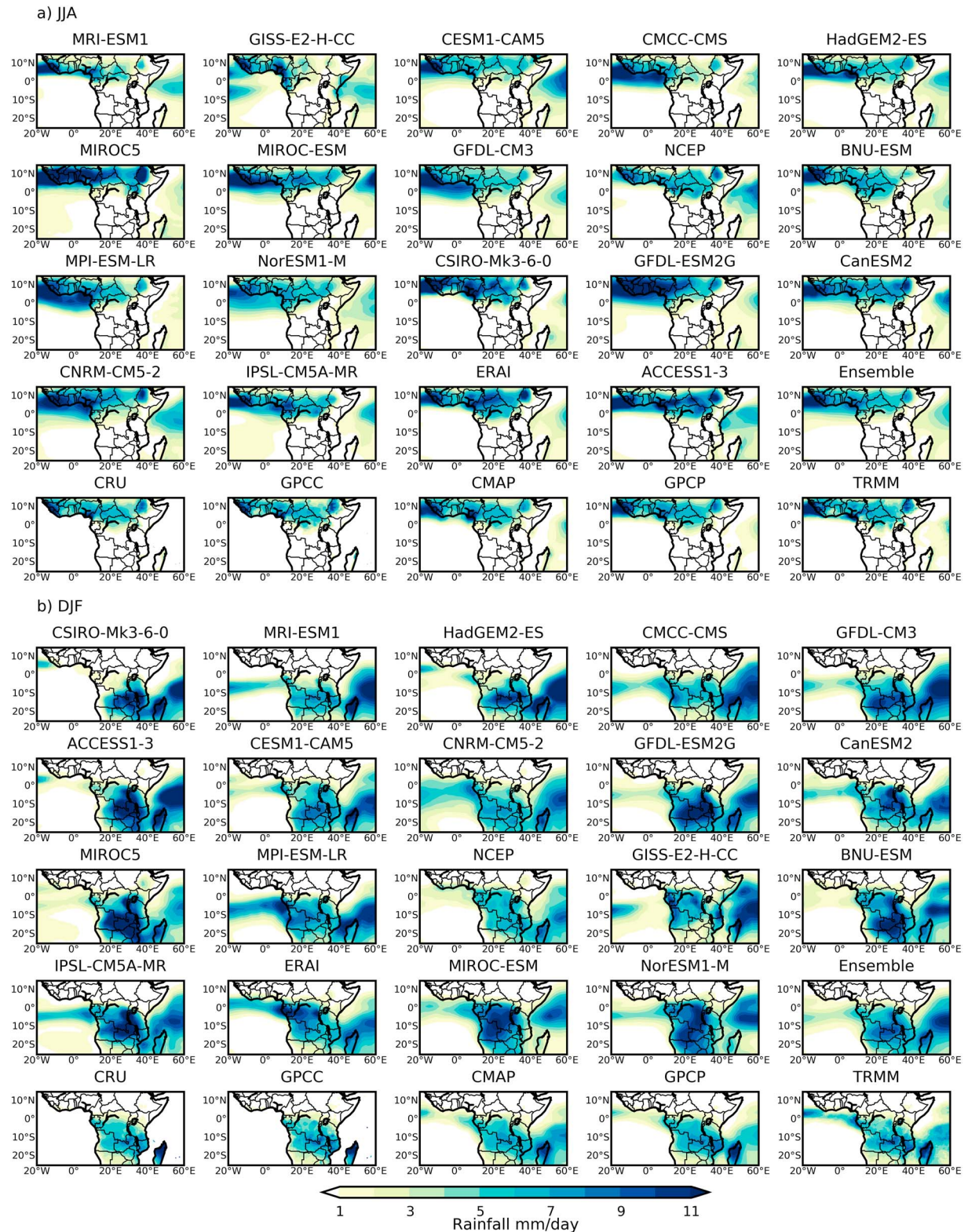


Figure 6. As for Figure 4 but for (a) JJA and (b) DJF.

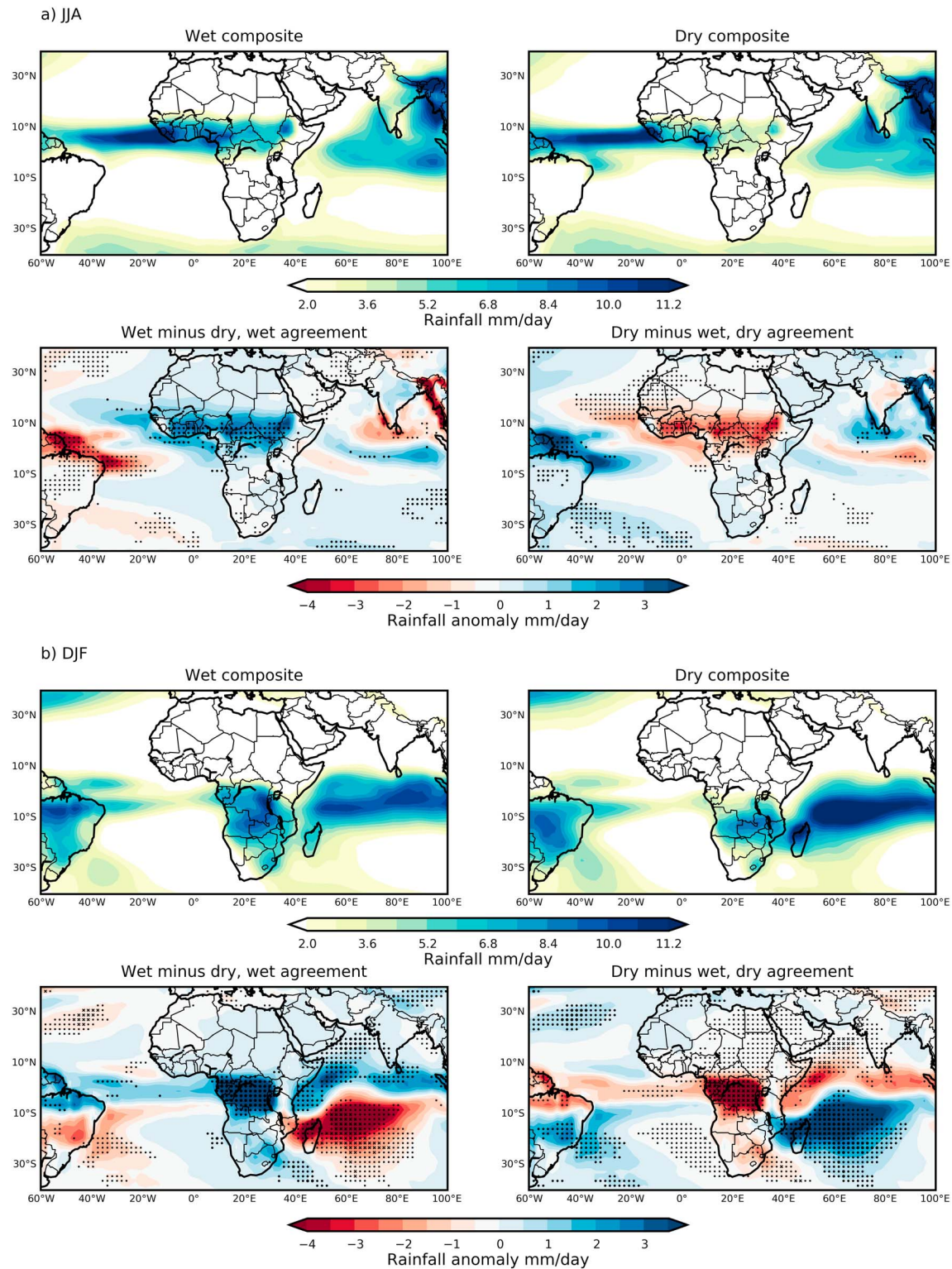


Figure 7. As for Figure 5 but for (a) JJA and (b) DJF.

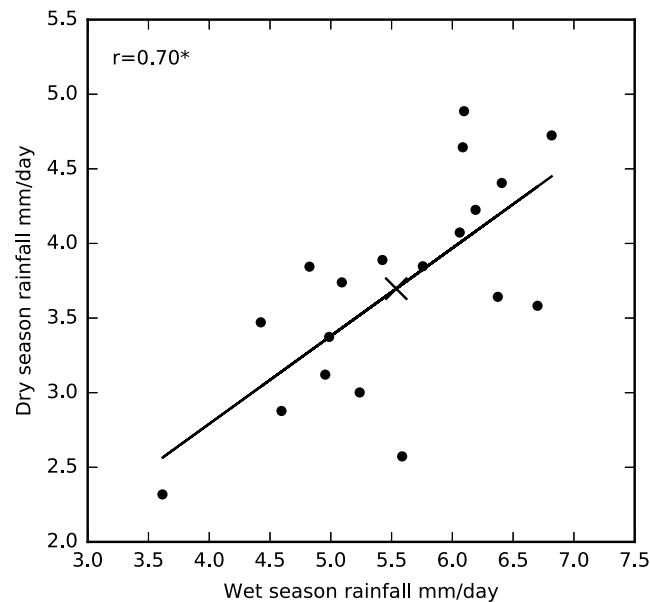


Figure 8. Relationship between the long-term mean (30 year) rainfall (mm d^{-1}) in the wet seasons (MAM and SON mean) and dry seasons (JJA and DJF mean) for individual data sets X indicates the ensemble mean.

4. Moisture Flux Convergence

In light of the disparities in rainfall magnitude and distribution between models, and given the paucity of observed rainfall data with which to confront models, alternative strategies must be adopted to assess model climatology and establish processes of importance for the Congo region. It follows that given the importance of the CMIP5 data set in the development of future climate projections, such a process-based analysis may turn out to be crucial in isolating climate projections which are based on realistic representations of the present climate.

Moisture flux (q_{flux}) convergence is a key aspect of the hydrological cycle in tropical regions [Burde *et al.*, 1996; Pokam *et al.*, 2012]. Previous research indicates that the magnitude, location, and height of q_{flux} convergence is related to rainfall [Washington *et al.*,

2013; Yin *et al.*, 2013] and could help establish the credibility of particular models or model groups. These studies suggest that relatively wet (dry) models may experience higher q_{flux} convergence (divergence) than drier (wetter) models at particular levels, related to branches of the large-scale and regional-scale circulations. If the same can be established for the Congo, the credibility of individual model rainfall could be assessed with reference to moisture flux climatology, which, as a dynamic field rather than a highly parameterized one, is a better constrained variable in the models than rainfall. Thus, far research has focussed on this relationship in wet seasons in the Congo in reanalyses. The following section assesses the relationship between rainfall and q_{flux} convergence for all seasons across the CMIP5 ensemble.

4.1. Relationship to Rainfall

Long-term seasonal means were calculated for q_{flux} convergence over the domain 5°E to 35°E and 10°S to 10°N , at 700 hPa and 850 hPa. Individual levels are chosen, as opposed to column-integrated moisture flux convergence, following Pokam *et al.* [2012], who determined that the wet seasons feature strong moisture flux convergence at these particular levels and that flux at these levels appears strongly related to branches of both the local- and large-scale circulation. Moisture flux convergence is given by $q_{\text{conv}} = -1 \left(\frac{dq_u}{dx} + \frac{dq_v}{dy} \right)$. Thus, positive (negative) values denote q_{flux} convergence (divergence).

The relationship between mean q_{flux} convergence and rainfall at 700 and 850 hPa for the model ensemble is shown in Figure 10. Due to large amounts of missing data at 850 hPa, CSIRO-Mk3-6-0 is excluded from the analysis at this height. All seasons feature positive correlation with rainfall at both 850 hPa and 700 hPa such that wetter (drier) models in the ensemble are characterized by higher convergence (divergence); the only season in which it is not a significant relationship is JJA at 850 hPa (Figure 9a, red). The strongest overall correlation is in DJF at 850 hPa ($r = 0.81$), though it is also highly significant at 700 hPa ($r = 0.79$). JJA and SON also feature their strongest positive relationship at 850 hPa ($r = 0.66$ and $r = 0.71$, respectively), the latter of which concurs with the finding of Pokam *et al.* [2012] that this pressure level is where moisture convergence most influences rainfall in SON. MAM is the only season to have its strongest relationship with rainfall at 700 hPa ($r = 0.70$), also in agreement with Pokam *et al.* [2012]. As expected, models are mostly convergent at 850 hPa, while at 700 hPa the spread of models straddles convergence and divergence. At 700 hPa models in SON have slightly higher convergence and rainfall than MAM, which may account for the tendency of SON to be slightly wetter than MAM.

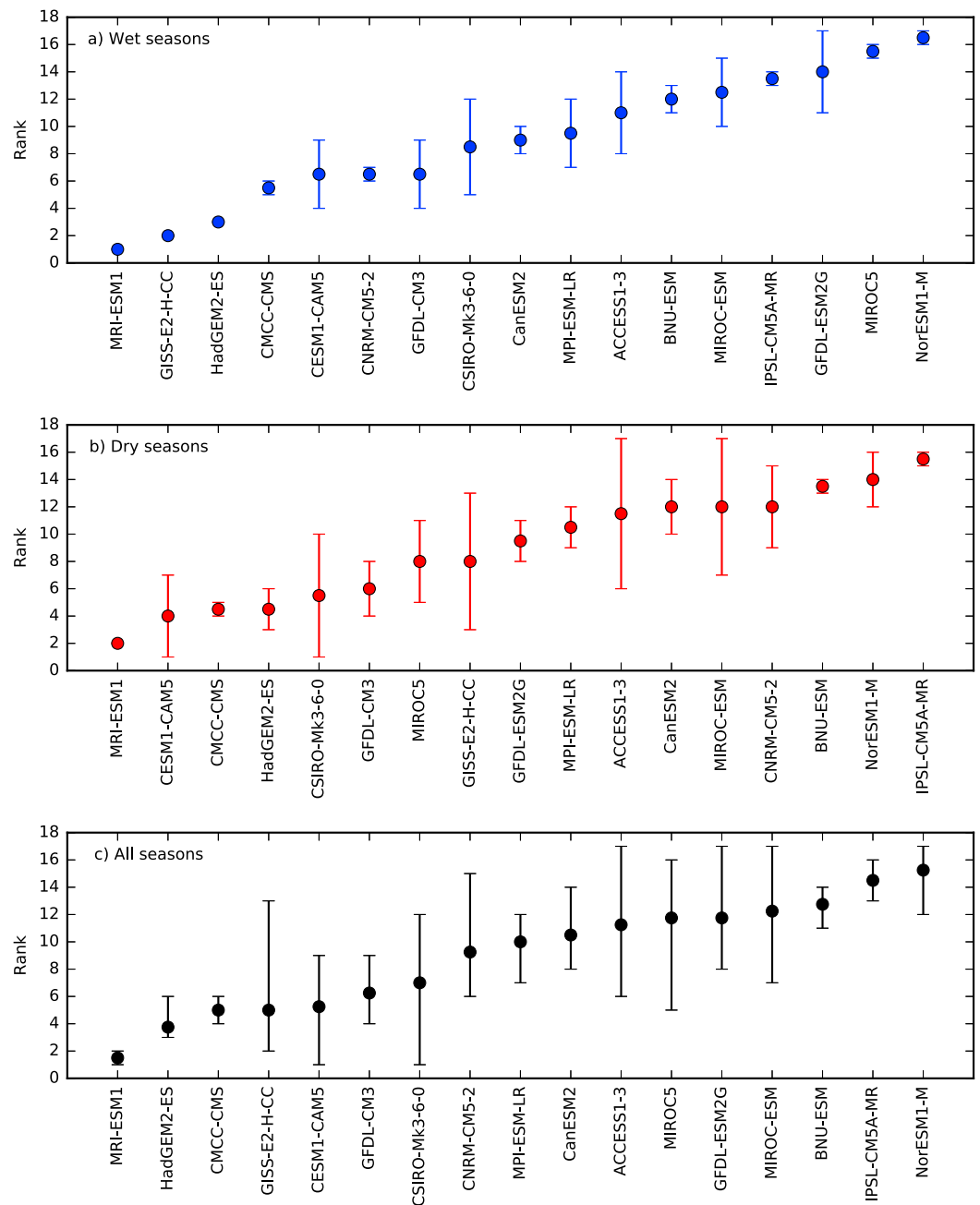


Figure 9. Average long-term mean (1971–2000) rainfall rank of CMIP5 models and reanalysis data sets for (a) wet seasons (MAM and SON), (b) dry seasons (JJA and DJF), and (c) all seasons. Rank 1 is the driest model; rank 17 is the wettest model. Circle denotes the mean rank. Solid lines denote the range in ranks each model occupies for the subset of seasons.

The qflux convergence metric combines wind convergence, in situ specific humidity (q), and moisture advected from surrounding regions [Pokam *et al.*, 2012]. To confirm that qflux convergence is more closely linked to rainfall than u , v , and q individually, similar correlation analysis is conducted for each constituent component (Table 3). At 850 hPa the combined role of specific humidity and wind convergence (qflux convergence) exhibits the strongest and most significant relationship with rainfall in all seasons. At 700 hPa, MAM, SON, and DJF also show the strongest relationship between rainfall and qflux convergence, while JJA only features a significant relationship with wind convergence. As a dry season this might be expected, as levels of q are much lower. This reinforces the importance of analyzing qflux convergence as a potential control on rainfall at these heights.

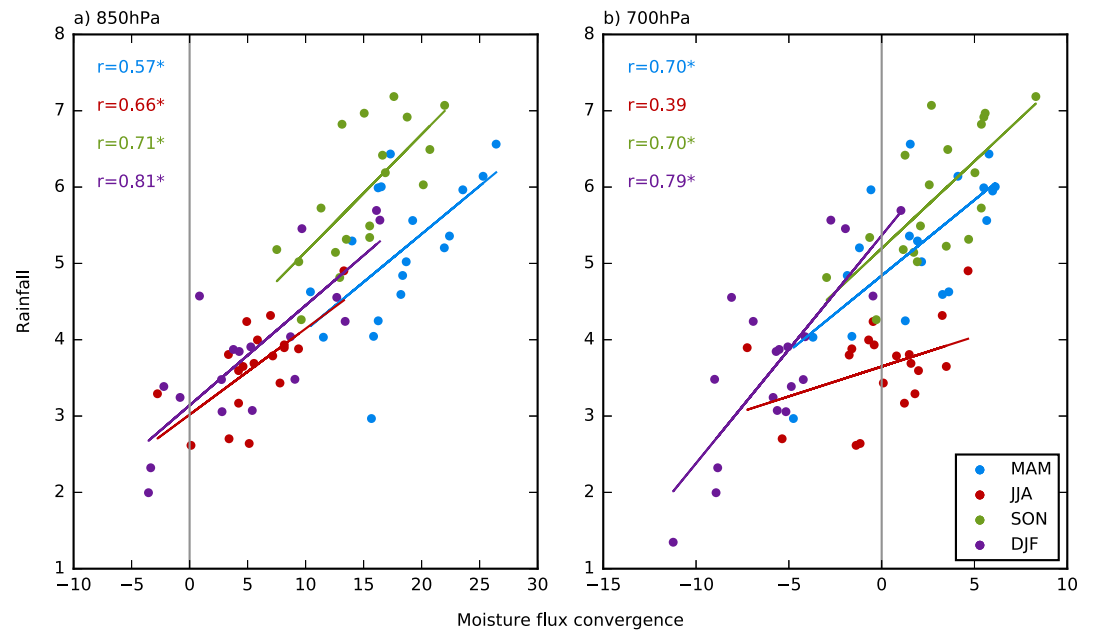


Figure 10. Long-term mean (1971–2000) moisture flux convergence ($10^9 \text{ kg kg}^{-1} \text{ s}^{-1}$) and rainfall (mm d^{-1}) at (a) 850 hPa and (b) 700 hPa for CMIP5 models and reanalyses data.

4.2. Wet and Dry Model Differences

Figure 11 shows the difference in long-term (30 year) mean qflux convergence between the five wettest and driest models in each season, overlain with the difference (wet minus dry) vectors of qflux. Only significant vectors (based on the agreement metric) are shown. Comparison with wet and dry model composites (supporting information, Figure S1a) allows an understanding of the direction of difference between the two subsets of models. In MAM at 850 hPa (Figure 11a), wet models feature more convergence over the majority of the basin than dry models, although dry models experienced greater convergence in the northeast corner of the domain (which is the location of maximum rainfall in dry models, as seen in Figure 5a). The causes of this difference in overall convergence appear twofold: first, wet models experienced greater qflux from the eastern boundary of the basin (from the Indian Ocean), and second, wetter models feature influx on the western boundary of the basin between 0° and 5°N , whereas dry models feature outward flow at this boundary. In wet models this inward flux is due to the recurvature of air as it crosses the equator; this does not feature in dry models (supporting information, Figure S1a). A similar pattern is evident in SON, where greater influx is evident at the western boundary. In both wet seasons, wet models also feature higher divergence than dry models in the far east of the basin.

At 700 hPa strong differences remain between wet and dry models (Figure 11b). In MAM, SON and JJA wet models feature anomalous inflow at the western boundary of the basin; the composites show that

Table 3. Correlation (r Value) Between Model Congo Basin Rainfall and (a) Specific Humidity, (b) Wind Convergence, and (c) qflux Convergence at 850 hPa and 700 hPa, in the Long-Term Mean

	850 hPa			700 hPa		
	q	Wind Convergence	qflux Convergence	q	Wind Convergence	qflux Convergence
MAM	0.22	0.33	0.57*	0.33	0.62*	0.70*
JJA	−0.07	0.58*	0.66*	0.09	0.49*	0.38
SON	−0.006	0.69*	0.71*	−0.07	0.64*	0.70*
DJF	0.75*	0.68*	0.81*	0.57*	0.78*	0.79*

*Significance at 95%. Bold indicates the highest correlation coefficient for each season and pressure level.

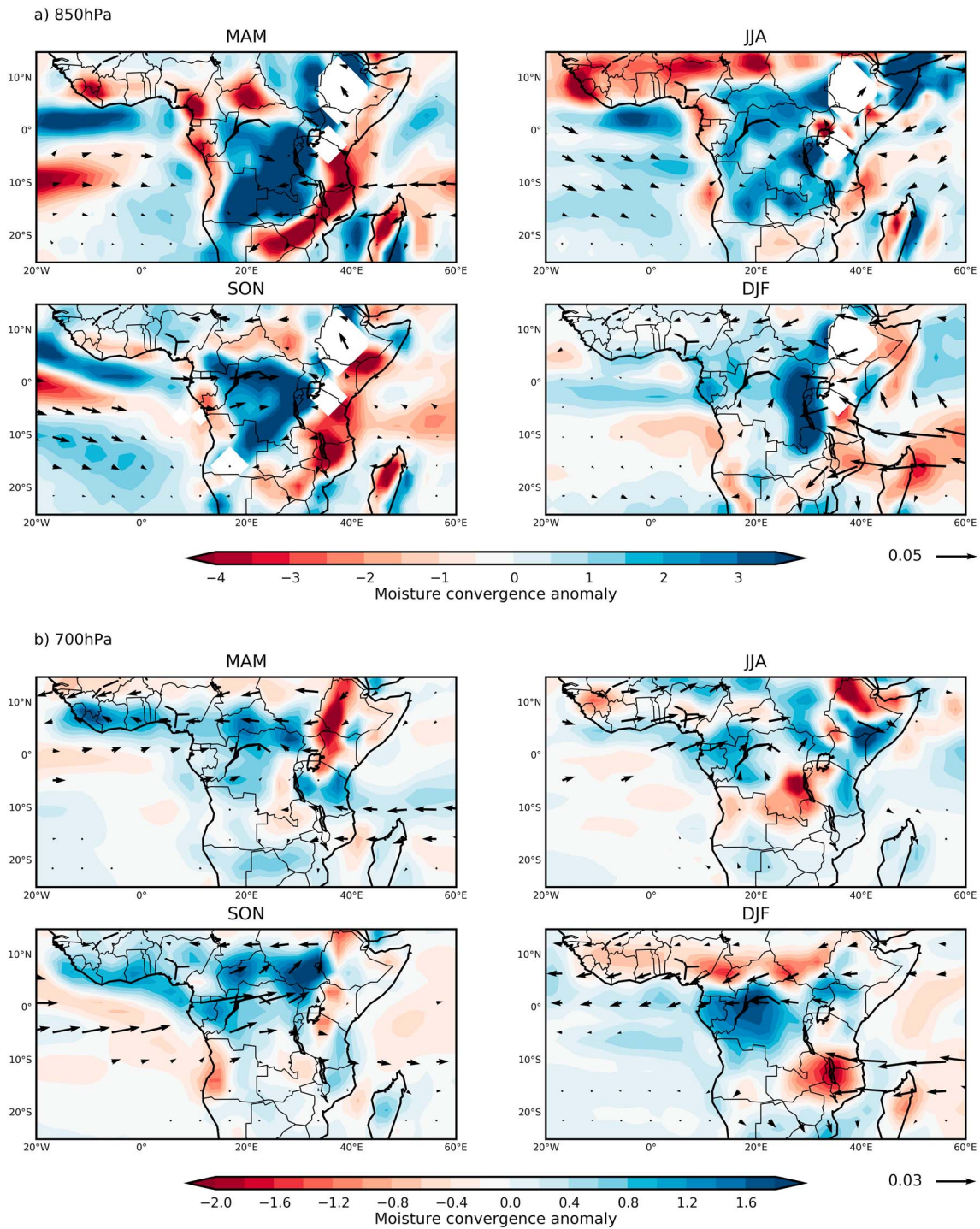


Figure 11. For (a) 850 hPa and (b) 700 hPa: Difference in moisture flux convergence (shaded; $10^8 \text{ kg kg}^{-1} \text{ s}^{-1}$) and moisture flux (vectors; $\text{kg kg}^{-1} \text{ m s}^{-1}$) between composite of five wettest and five driest models in each season. Only vectors which are significantly different between the wet and dry ensembles (using the agreement metric described in section 3.2.1) are shown.

this is due to less moisture-laden air leaving the basin in wet models than dry (supporting information, Figure S1b). This results in greater convergence over the basin in wet models. In DJF, wet models feature increased influx from the eastern boundary, whereas dry models feature significant outflow toward the southeast of the basin.

5. Spatial Limits to the Convergence-Rainfall Relationship

5.1. Location of Convergence Maxima

Section 3.2 highlights the distinct east versus west rainfall distributions that characterize many models. If local convergence is a controlling factor on the location of rainfall, we might expect the rainfall and convergence maxima (at important levels) to collocate. To this end, Figures 12 and 13 show the location of top 20% of rainfall values (blue) and convergence (red), with areas of overlap of the distributions highlighted (pink). The location of the maximum value is designated by a star (rainfall) and a cross (convergence). The pressure level at which each season featured the highest correlation is shown (850 hPa for MAM and SON and 700 hPa for JJA and DJF; other heights are shown in supporting information, Figures S2 and S3).

Most models feature some overlap between the location of top 20% of rainfall and convergence. Several data sets in MAM at 700 hPa (e.g., MIROC5, ACCESS1-3, NCEP, and IPSL-CM5A-MR) (Figure 12a) show large areas of overlap on land, and the maximum value of each are very close. Others show less significant overlap but still collocate the maxima (e.g., ERAI). There is no distinct pattern, however, between models which do and do not collocate. This is affirmed by a correlation analysis on both the latitudinal and longitudinal locations of the maxima, which shows insignificant relationships at both heights for MAM. Nevertheless, five data sets feature very similar locations of rainfall and convergence maxima. In SON (Figure 12b) three of the same data sets show collocating maxima (ACCESS1-3, IPSL-CM5A-MR, and ERAI), in addition to MRI-ESM1 and CSIRO-Mk3-6-0. There also appears to be broader agreement in the general location of the top 20% values, with larger areas of overlap than in MAM.

For the dry seasons it must be noted the boundaries of the chosen domain (10°N and 10°S) bisect the zone of tropical convection. This could influence the location of maximum rainfall and convergence, depending on the latitudinal extent of the rainfall band in each model. In JJA at 850 hPa (Figure 13a), there are two broad zones of rainfall maxima in most models, so a secondary maximum (smaller star) is plotted as well. There is very little agreement between the location of either rainfall maxima, which tend to be in the northwest and north central zones of the domain, respectively, and the convergence maxima, which is in the east central zone of the domain. These patterns are quite consistent across models and do not seem to be related to the relative wetness or dryness of the model. In DJF at 850 hPa (Figure 13b) eight models feature near collocation of maxima, in the southeastern quarter of the domain. These all span the wetter half of the models; near collocation does not occur in any of the eight driest models.

5.2. Spatial Limits at the Subdomain Scale

Section 5.1 indicates that the relationship between rainfall and convergence amongst models is strong at the basin scale. This section further quantifies the spatial limits of this relationship by testing its significance in the four subdomains (northwest (5°E, 20°E, 0°, 10°N), northeast (20°E, 35°E, 0°, 10°N), southwest (5°E, 20°E, 10°S, 0°), and southeast (20°E, 35°E, 10°S, 0°)).

5.2.1. Wet Seasons

At the domain scale, MAM features the strongest positive relationship at 700 hPa ($r = 0.70$). This is dominated by relationships in the northeast and northwest subdomains, with a smaller but still significant relationship in the southeast (Figure 14b). Figure 14b indicates that the northern half of the domain is dominated by divergence in this season. Thus, the overall relationship at 700 hPa appears to be dominated by a more divergence/less rainfall relationship. At 850 hPa, the domain-scale positive relationship ($r = 0.57$) is dominated by strong correlation in the southwest and southeast subdomains (Figure 14a), the latter of which is dominated by convergence.

At the most significant height (850 hPa) in SON, the overall positive relationship ($r = 0.71$) is dominated by the western domains, with a smaller but significant relationship in the southeast. The largest r value, and the greatest gradient of the correlation relationship, is in the northwest, which overwhelmingly features convergence. This supports the findings in section 4.2, which show that wetter models feature much greater flow into the western half of the basin than dry models (Figure 11), contributing to greater convergence in this region. The southwest features divergence in most models; this is a well-defined feature in the southwest coast in all individual climatologies at this height (supporting information, Figure S1). At 700 hPa, all subdomains feature a significant relationship between rainfall and qflux convergence (Figure 14b). Unlike in MAM, the two northern domains predominantly exhibit convergence, whereas the southeast domain, which

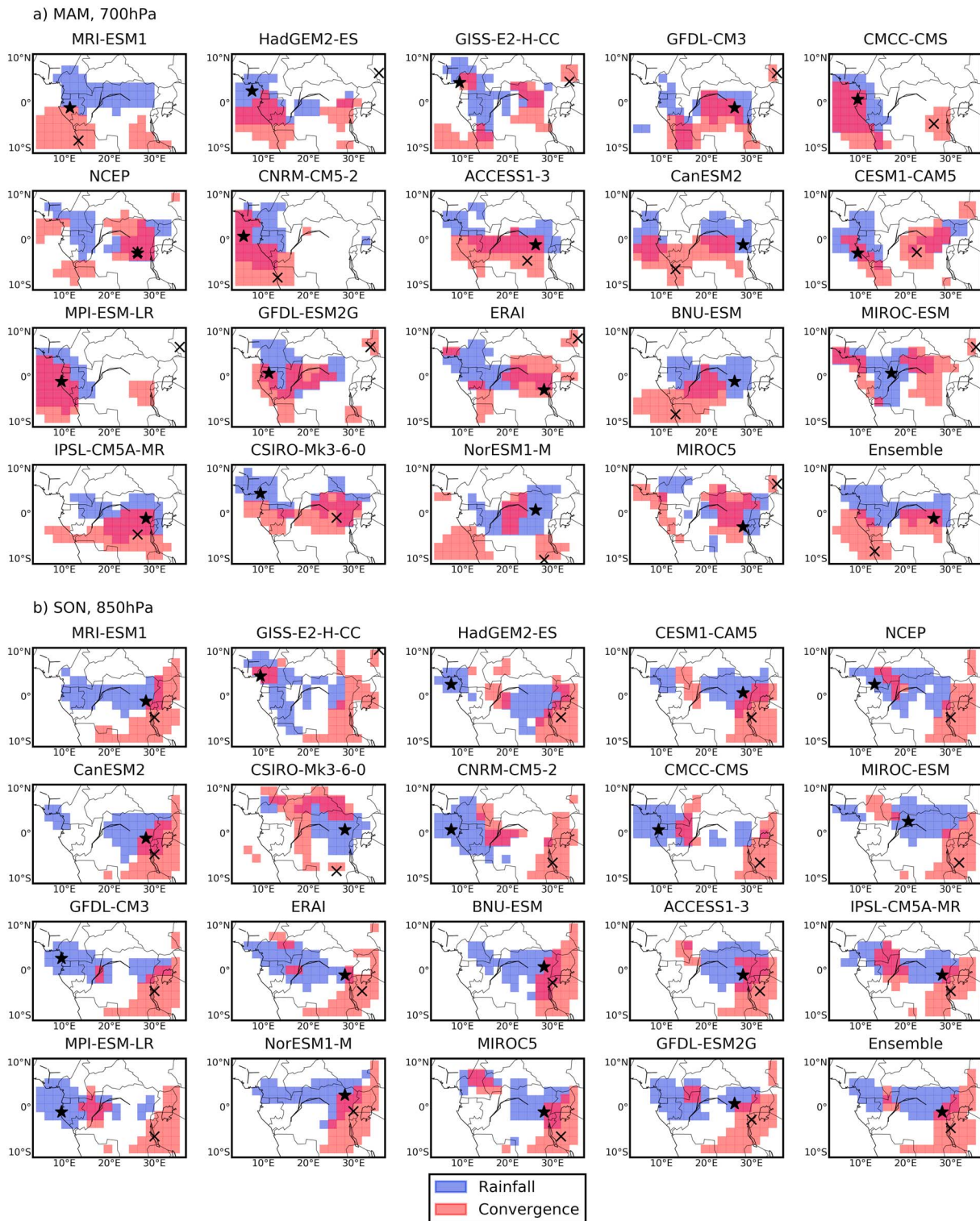


Figure 12. Location of top 20% of rainfall values (blue), moisture flux convergence values (red), and areas of overlap (pink) in (a) MAM at 700 hPa and (b) SON at 850 hPa. The location of maximum rainfall (convergence) is denoted by a star (cross).

exhibits the weakest (though still significant) relationship, is dominated by divergence. The largest r value, and the greatest gradient of the correlation relationship, is in the southwest of the domain, which overwhelmingly features convergence. This supports the findings in section 4.2, which show that wetter models

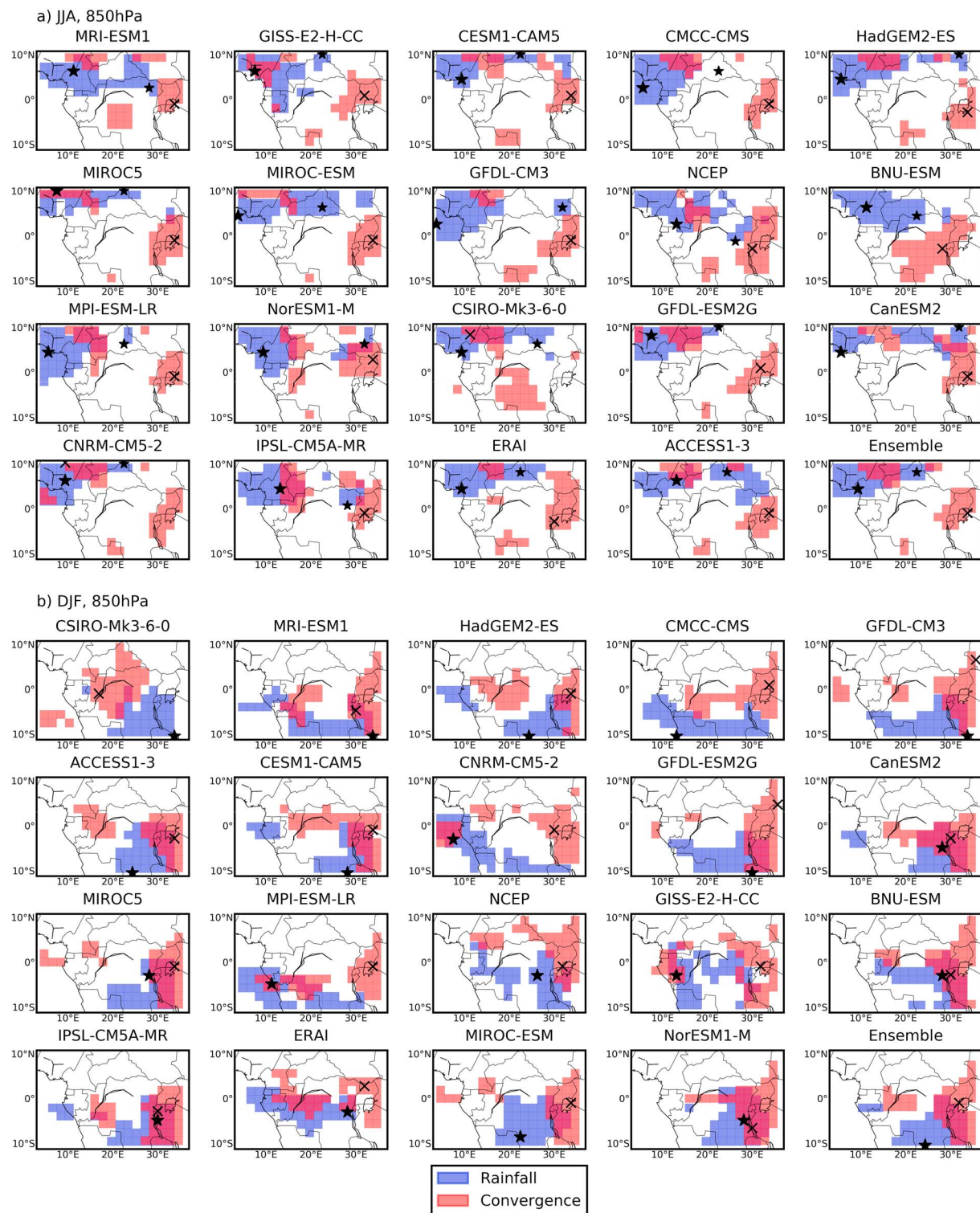


Figure 13. As for Figure 12 but for (a) JJA at 850 hPa and (b) DJF at 850 hPa.

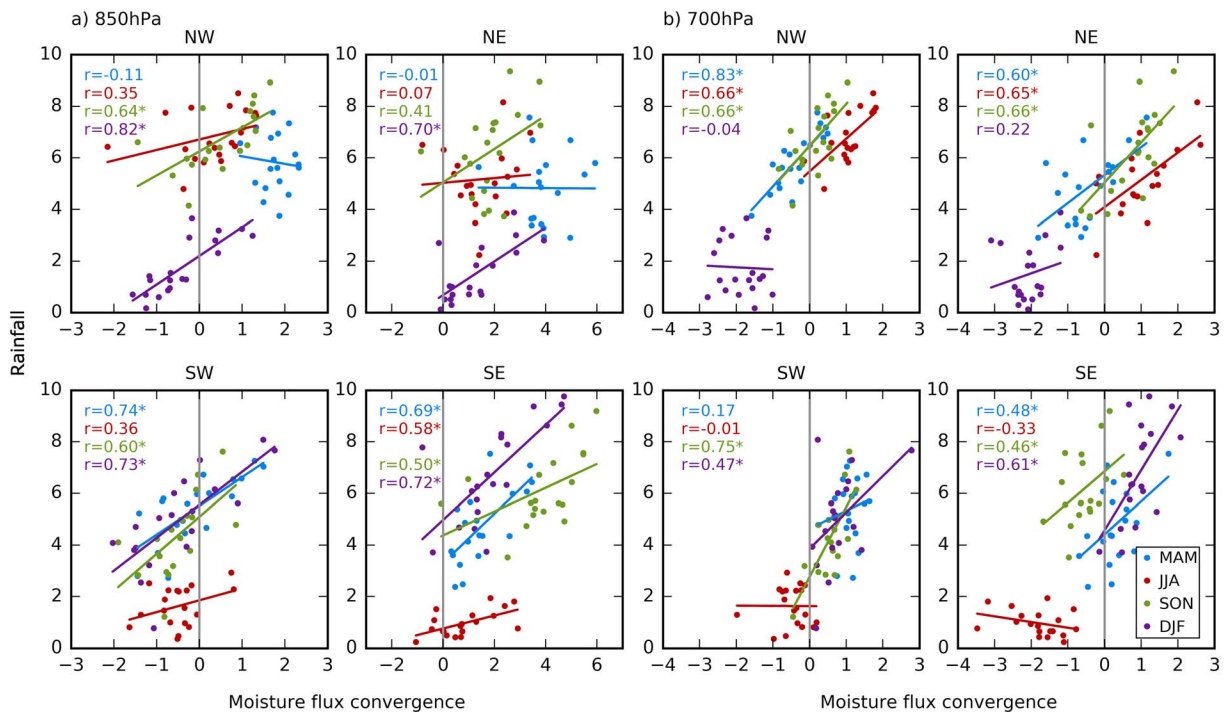


Figure 14. Relationship between long-term mean (1971–2000) moisture flux convergence ($10^8 \text{ kg kg}^{-1} \text{ s}^{-1}$) at (a) 850 hPa and (b) 700 hPa and rainfall (mm d^{-1}) for CMIP5 models, ensemble mean and two reanalysis data sets in the northwest (top left), northeast (top right), southwest (bottom left), and southeast (bottom right).

feature much greater flow into the western half of the basin than dry models (Figure 11b), contributing to greater convergence in this region.

5.2.2. Dry Seasons

Both dry seasons feature their strongest domain-scale relationship at 850 hPa. JJA only features a significant positive relationship in the southeast at this height ($r = 0.58$) (Figure 14a). Models here are mostly convergent but weakly so relative to all other seasons and still experiencing very low rainfall totals. At 700 hPa, JJA experiences strong positive correlation in the two northern domains, which are the wet, convergent regions in this season. However, it does not feature a significant relationship at 700 hPa for the whole domain; this suggests that the relationship is spatially limited to the zone of tropical convection in the northern half. This may mean that the relationship in JJA is less useful when determining differences between models in the southern half of the basin, a region in which rainfall is already marginal in this season.

In DJF at 850 hPa, strong positive relationships are found in all subdomains (Figure 14a). In the eastern two subdomains these are dominated by convergence. The southeast domain is also where several wet models feature their maxima of both rainfall and convergence (Figure 13b). In the western domains the models are split between average divergence and convergence. At 700 hPa DJF only exhibits significant relationships in the two southern domains, in particular in the southeast. This affirms the important role of flux into the basin from the Indian Ocean, as shown in Figure 11b. In the northern domains there is no relationship between qflux and rainfall. This concurs with the pattern seen in JJA; at 700 hPa, the relationship is dominated by the region under the band of tropical convection, whereas the dry, divergent regions of the domain do not feature a relationship between the two.

6. Origin of Water Vapor Transport

6.1. Direction of Water Vapor Transport Into the Basin

The preceding sections indicate that while the relationship between qflux convergence and rainfall is significant at the domain scale, there are particular regions which contribute most to the total amounts of convergence or divergence in the region. It thus follows that particular branches of the larger regional circulation may be more or less influential depending on the season and height and, if these can be identified, could

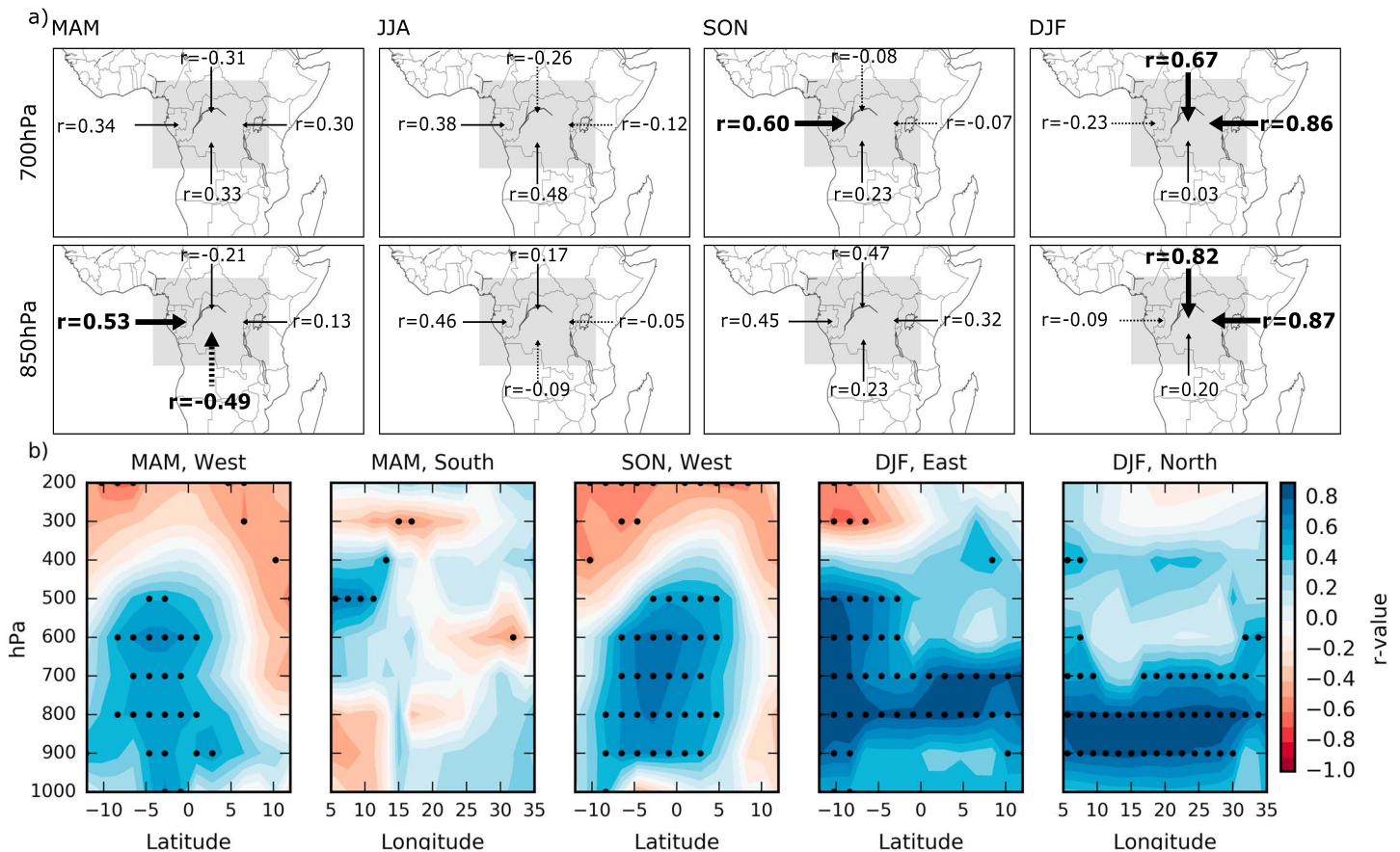


Figure 15. (a) Schematic showing the correlation coefficient between long-term mean rainfall over the basin and moisture (q_{flux}) entering the basin across the northern, eastern, southern, and western boundaries at 850 hPa and 700 hPa. Large arrows and bold text denote r values significant at the 95% level. Dashed arrows indicate a negative relationship. (b) Latitude/height and longitude/height cross sections for flow across boundaries which feature significant correlations. Individual vertical grid locations which feature significant correlations are stippled.

be used to further constrain model rainfall values. In the long term, this relationship could lend itself to an observational campaign on the fringes of the Congo. While long-term monitoring of rainfall within the basin itself is difficult, given its remoteness and the political tensions in the region, it remains a possibility that observing dynamical fields such as q_{flux} as it enters the basin may serve as a way of constraining climate models.

To that end, the average gridbox moisture flux into the basin is calculated over all four boundaries: north (10°N), south (10°S), east (35°E), and west (5°E). This is correlated with rainfall over the basin, and the results are shown schematically in Figure 15a (where large arrows indicate significant relationships). Figure 15b shows the latitude/longitude-height cross section of these correlations for significant boundaries.

At 850 hPa in MAM there is a significant relationship between moisture entering the basin from the west and rainfall. This affirms previous results suggesting that the recurvature of air at the equator is greater here for wet models than dry models in MAM (supporting information, Figure S1a); therefore, wetter models receive greater inflow across this boundary. Figure 15b highlights the dominant role of low-to-middle level flow. There is also a negative correlation at the southern boundary, whereby models receiving greater flux over this boundary experience less rainfall. This could be a result of stronger southeasterly flux in dry models, which leaves the basin via the eastern boundary and experiences less convergence than in wet models (Figure S1). At 700 hPa, no boundaries feature a significant positive relationship. However, analysis of individual model values (not shown) suggests that there are two extreme outliers that are disproportionately impacting the relationship in MAM. CSIRO-Mk3-6-0 has the lowest q_{flux} value yet the third highest rainfall value. Further investigation indicates that CSIRO-Mk3-6-0 features anomalously low inflow from east between 700 hPa and

500 hPa (compared to other models) but anomalously high influx from the south at 600 hPa and 500 hPa, where most models exhibit net outflow. The height at which this anomaly occurs suggests that the large-scale dynamical circulation (i.e., wind convergence) is dominating the relationship in this model. Analysis of both moisture convergence and wind convergence plots (not shown) confirms the dominant role of large-scale circulation in CSIRO-Mk3-6-0's anomalies, in the absence of the role of specific humidity at these heights. The second anomalous model, MRI-ESM1, is consistently dry in all seasons, despite having near-average amounts of convergence. If both models are removed from the analysis, the relationship strengthens considerably more than expected from the removal of two degrees of freedom and becomes significant ($r=0.57$).

In SON the only significant relationship between rainfall and qflux entering the basin is at 700 hPa from the west of the basin. This coincides with the region of greatest difference between wet and dry models (Figure 11b), where wet models show greater inflow over this boundary, as in MAM. This concurs with previous work by Pokam *et al.* [2012, 2014] which suggests that low-level westerly flow from the Atlantic is a dominant source of moisture in SON, and Figure 15b highlights the dominant role of low-to-middle level flux. At 850 hPa, SON exhibits no significant relationships, though it must be noted that at 850 hPa several models feature some missing data; in addition, Figure 15b shows that for the southern part of the boundary, the relationship remains significant down to 900 hPa.

JJA shows no significant correlation between the variables; this may be due to threshold behavior in JJA, where the total provision of moisture is not consistently high enough to exceed thresholds in thermodynamic instability, resulting in low rainfall across the majority of the basin. DJF exhibits positive, significant relationships between qflux and rainfall over the northern, eastern, and southern boundaries at 850 hPa, with the most significant flux coming from the east ($r=0.85$). This strong relationship extends upward to 700 hPa ($r=0.86$), indicating that the amount of flow at low to middle levels entering the basin from the east is strongly linked to how much rainfall the basin experiences as a whole, and in particular the eastern side (Figure 14a). Again, Figure 15b highlights the dominance of the low to middle levels in this relationship. This result complements an assessment of individual model climatologies (not shown) which show strong influx into the basin from both the northeast and southeast from the Indian Ocean. The reversal of the land-sea thermal contrast in Northern Hemisphere winter, and the associated northeasterly flow from the Indian subcontinent, is a likely source for this flow.

6.2. Possible Influences on Water Vapor Transport at Basin Boundaries

Figure 15 highlights the boundaries and heights at which moisture entering the basin is associated with rainfall. It is likely that these relationships are related to models' representation of the interaction between the regional and large-scale circulations. Figures 5 and 7 indicate that these circulatory differences may be related to model SST; there are significant differences between basin rainfall and ocean rainfall between wet and dry models. In order to determine the possible role of SST on basin rainfall, correlation analysis was performed between Congo Basin rainfall and SST at each grid box, across the suite of models (Figure 16). This indicates that correlations exist between rainfall over the basin and SST in surrounding oceans and that some of these colocate with regions of precipitation differences between wet and dry models (Figures 5 and 7).

SST biases in both the Atlantic and Indian Oceans have been well documented [e.g., Wang *et al.*, 2014]. For example, strong warm biases in the tropical and the southeast Atlantic have been a persistent feature of coupled models [Davey *et al.*, 2002; Richter and Xie, 2008] and have been attributed to problems in both the atmospheric and oceanic model components, as well as the ocean-atmosphere feedbacks in coupled models [e.g., Wahl *et al.*, 2009; Richter *et al.*, 2012; Xu *et al.*, 2014]. It is well established that SSTs in this region influence West and equatorial African rainfall [Hirst and Hastenrath, 1983; Nicholson and Entekhabi, 1987; Camberlin *et al.*, 2001; Todd and Washington, 2004], and Figure 16 shows that this bias is strongly related to basin rainfall in DJF. Most recently, Cook and Vizy [2015] have determined that when Gulf of Guinea SSTs are anomalously warm, low-level westerly flow into the basin is increased, feeding the lower branch of a Walker circulation over the basin and resulting in higher rainfall. Pokam *et al.* [2014] have also linked differential heating of land and ocean to the formation of low-level westerlies in reanalysis data. A logical extension of this work is to assess the extent to which SST biases can account for differences in model rainfall via circulation patterns. This is the subject of a follow-up paper in preparation by the authors.

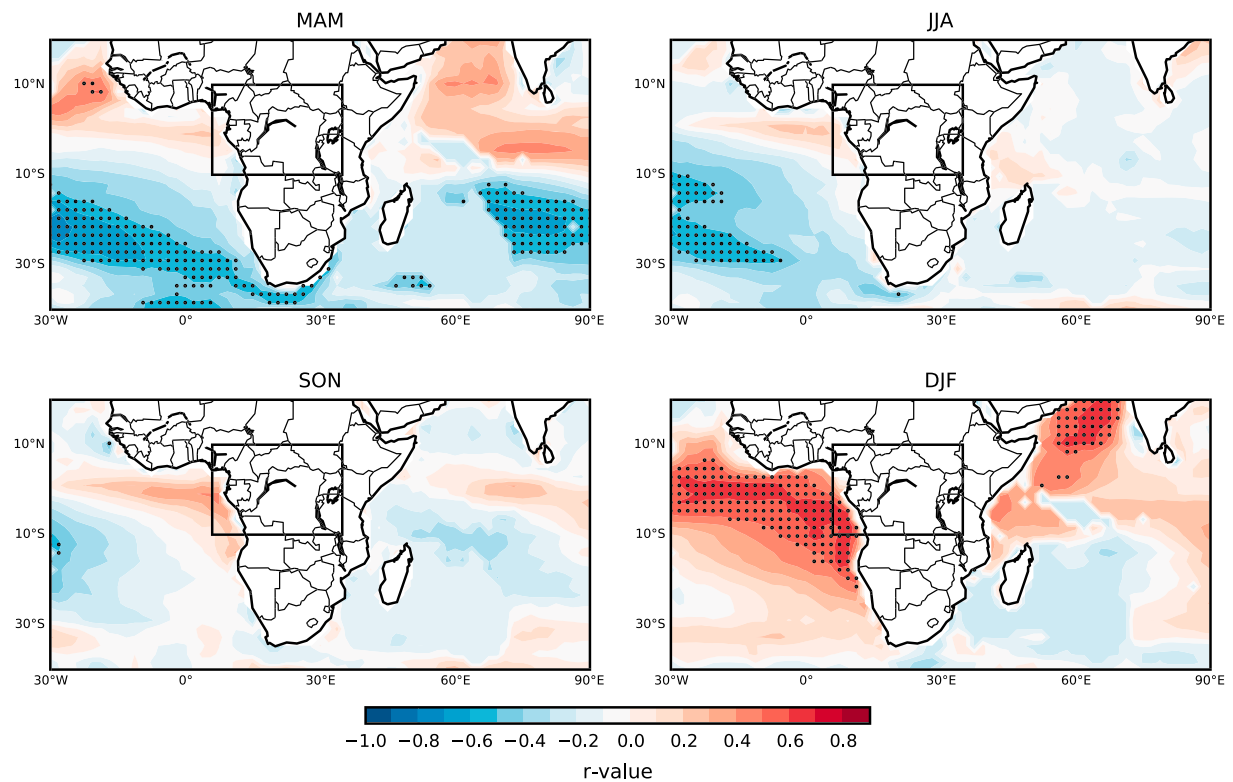


Figure 16. Relationship between long-term mean basin rainfall (5°E–35°E, 10°S–10°N; mm d⁻¹) and SST bias (°C) at each gridbox, across 17 CMIP5 models.

Local-scale factors, such as model representation of topography, may also interact with the large-scale circulation and contribute to some of the differences in moisture flux at the Congo Basin boundaries. A full analysis of the influence of topography will require an experimental setup of a varying resolution climate model; however, some insight can be gained from the low-resolution models used here. Figure 17a shows the land surface height of a transect across the basin at the equator in 10 models (those in our sample which provided orography data). At the point of maximum difference (0°, 36°E; grey dashed line), a correlation analysis was performed between land surface height and rainfall, for all seasons. Significant negative correlations were returned for MAM ($r = -0.65$, Figure 17b) and SON ($r = -0.65$, not shown), showing that wetter (drier) models tend to have lower (higher) surface altitude on the eastern boundary of the basin. No significant results were returned for JJA or DJF.

To determine whether qflux totals are also related to topography, a second correlation analysis was conducted between land surface height and qflux into the basin at 700 hPa from the east. A significant negative correlation was returned for MAM (Figure 17c), suggesting that higher topography in drier models blocks some moisture transport from the east and may be one cause of model divergence. In SON, the analysis did not return a significant correlation, indicating that for this season the relationship between rainfall and topography is more complex. Further analysis of the role of topography in model rainfall differences is planned for future work.

7. Discussion

This study comprises an analysis of CMIP5 rainfall climatologies for the Congo Basin. As expected from the results of Washington *et al.* [2013], there is little agreement amongst model rainfall magnitude, with some monthly totals differing by a factor of 5. The spatial distribution of rainfall also varies substantially across models; in some seasons, there is a tendency for either strong eastern or western rainfall maxima which are often consistent within models. Controls on rainfall are likely to be distinct between these two groups, highlighting the importance of intermodel comparison for identifying these differences. This finding has implications for the use of multimodel ensemble means in climatological analyses. MME means

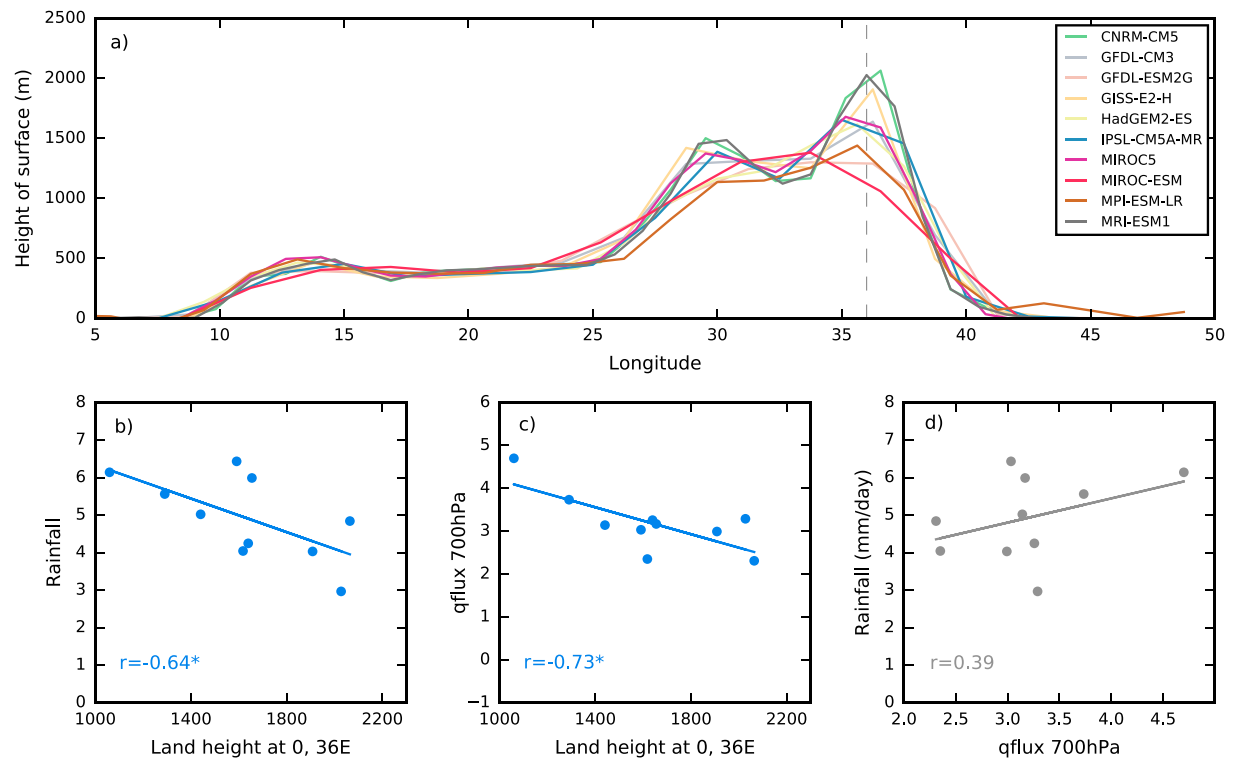


Figure 17. (a) Longitude/height (m) cross section of land surface height for 10 models at the equator. The relationship in MAM only between (b) land surface height (m) at 0°, 36°E and rainfall (mm d^{-1}); (c) land surface height at 0°, 36°E and qflux into the basin at 700 hPa at 35°E ($10^2 \text{ kg kg}^{-1} \text{ ms}^{-1}$); and (d) qflux from the east at 700 hPa and rainfall.

are frequently used as a “best estimate” of climatology, working on the principle that errors and uncertainties in individual models will be reduced by the averaging process [Hagedorn *et al.*, 2005; Palmer *et al.*, 2005; Tebaldi and Knutti, 2007]. However, the strongly opposite distributions between many models (Figures 4 and 6) cancel out when averaged, resulting in ensemble mean plots that feature homogenous, low-magnitude rainfall across large areas of the domain. Unlike the ensemble mean, there are few models in any season which show a central and homogenous rainfall distribution, suggesting that the ensemble mean is not representative of Congo rainfall climatology. If a homogenous area of rainfall is representative of the observed, then it is not a distribution captured by any one model.

Recent approaches in model evaluation have encouraged the use of process-based assessments to determine the credibility of individual models. Moisture flux convergence has been established to be a useful metric in constraining rainfall in the tropics and has here been applied to a range of data sets in the Congo. The relationship between qflux convergence and rainfall is positive and significant in all seasons and at both heights, bar JJA at 700 hPa. Again, excepting JJA at 700 hPa, this relationship is stronger than the individual relationships between the components of qflux convergence (specific humidity and wind convergence) and rainfall across the domain, indicating the significance of their combined role on rainfall climatology across models. Previous studies have shown that in the Amazon, another of the three global convective hot spots, coupled models which produce more realistic moisture convergence also simulate more realistic rainfall amounts and distributions [Yin *et al.*, 2013]. A similar relationship was found at the interannual scale for reanalysis data sets [Pokam *et al.*, 2012] where wet (dry) years featured stronger (weaker) moisture convergence. This result is therefore promising as a first step in determining the credibility of individual model rainfall climatologies, as the large-scale wind component of qflux convergence is better constrained in models than rainfall.

Results in section 3 support previous suggestions that SON is the primary wet season (e.g., Figure 3); nearly all models feature higher rainfall in SON than MAM. While differences between the two rainy seasons have been noted (e.g., Sandjon *et al.* [2012] notes that SON rains are shorter and less intense), there is no firm consensus on which season is wetter. It has been noted that rainfall is more intense in equatorial Africa during

seasons with African easterly jet (AEJ) development both sides of the equator [Nicholson and Grist, 2003] as the southern branch of the AEJ only fully develops in the second half of the year. Haensler et al. [2013] suggest that this might be the reason for higher rainfall in SON. Thus, the finding that SON tends to be wetter than MAM is consistent with a shared mechanism, such as the AEJ, acting amongst models. There are some differences in convergence climatologies which further agree with this. For example, while all models in both MAM and SON are convergent at 850 hPa, more models in SON are convergent at 700 hPa, and average convergence across models is higher than in MAM (Figure 10b). Higher convergence in SON might be accounted for by regional-scale circulation, for example, the presence of both branches of the AEJ in this season [Haensler et al., 2013]. Additionally, dry biases in models have been linked to excessive moisture divergence in the tropics and, thus, further suppression of rainfall [Yin et al., 2013]. The relationship between moisture divergence and rainfall may therefore involve positive feedbacks; this warrants further investigation, particularly in the dry seasons where divergence dominates.

These findings build on previous research conducted over the tropics and equatorial Africa on the relationship between thermodynamical mechanisms and rainfall. Collins et al. [2013] highlight that thermodynamic feedbacks within individual models may contribute to a “wet-gets-wetter/dry-gets-drier” mechanism, whereby enhanced water transport creates more convergence (divergence) in convergent (divergent) areas [Held and Soden, 2006]. Thus, feedbacks in hydrological variables might be the cause of consistent wetness/dryness of models across seasons. This indicates that an assessment of the SST/rainfall relationship in this region might be fruitful. Additionally, analysis of CMIP3 and CMIP5 data suggests that the rainfall response in convection zones is highly sensitive to spatial heterogeneities, which may include local moisture convergence feedbacks or the rate of moisture influx from surrounding regions [Chou et al., 2006; Neelin et al., 2006]. This research reinforces these findings, suggesting that the qflux/rainfall relationship could be used to differentiate models, in the absence of rainfall station data.

Despite a large-scale relationship between moisture convergence and rainfall over the basin, the relationship does not appear to have a strong spatial signal. In the wet seasons, there is no obvious relationship between the location of rainfall and convergence maxima. This suggests that while high moisture convergence may set up the conditions for convection, local controls (for example, surface heating, mesoscale convective organization, moisture cycling, and orography) most probably have a greater influence on the location of maximum rainfall. Further, the strong positive relationship between rainfall and qflux convergence observed at the domain scale is evident in some subdomains but not all. In MAM at 700 hPa, a significant correlation coefficient is present in subdomains which feature mean divergence and low rainfall (northeast and northwest). This might indicate that the local relationship in this season is subject to a threshold, below which the relationship between rainfall and qflux convergence does not hold up or is tempered by another variable. In SON at 700 hPa rainfall in all subdomains features a strong, significant relationship with moisture flux convergence; this suggests the presence of a large-scale control across the basin. JJA shows the opposite pattern to that in MAM at 700 hPa; the only statistically significant relationships are in the northern two domains in JJA, which are the wettest and most convergent. The domain as a whole does not feature significant correlation in JJA at 700 hPa, indicating that the relationship rapidly breaks down in the drier, southern half of the domain. DJF features strong positive relationships in all subdomains at 850 hPa. As in SON this suggests that the region is highly influenced by convergence across the basin in DJF.

Previous work indicates that moisture entering the basin at low levels from the west (SON) and east (MAM) is a key control on rainfall totals and variability in reanalyses [Pokam et al., 2012, 2014]. Figure 11 indicates that wetter models tend to experience greater flux across these two boundaries, and Figure 15a identifies the relative importance of these boundaries for different seasons. The amount of moisture entering the basin from the west at 700 hPa is highly related to rainfall in SON, and Figure 15b shows that for some latitudes this relationship extends in both directions in the atmospheric column. This relationship suggests a possible link to low-level westerlies and Atlantic influences, as found by Pokam et al. Additionally, once anomalous models have been removed, MAM features a relationship between low-to-middle level flux across the eastern boundary and rainfall over the basin as a whole (again in agreement with Pokam et al.). Figure 17 suggests that for this season, qflux from the east is in part influenced by model representation of topography. However, this relationship is complex or nonexistent for the rest of the year, which is perhaps expected as previous studies have found no simple relationship between rainfall and model resolution over this region [Washington et al., 2013; Moufouma-Okia and Jones, 2014]. DJF stands out as having the strongest relationships with qflux across

several boundaries, in particular the east and across the northeastern and southeastern corners of the domain. Pokam *et al.* [2012] suggest that this is related to the AEJ-N, which is located in the north of the basin during DJF, and is also likely related to northeasterly flow from the Indian subcontinent in this season.

8. Conclusions

This study is the most comprehensive assessment of the causes of model rainfall difference in the Congo. It utilizes the relationship between a dynamical variable and rainfall to determine the likely first-order causes for the relative differences between models. The following conclusions have been reached:

1. There is little agreement amongst CMIP5 model simulations of Congo rainfall. This has implications for the use of multimodel ensemble means for this region.
2. Moisture flux convergence has a strong relationship with rainfall (a) in all seasons and (b) at two different levels in the atmosphere.
3. The height in the atmosphere at which these relationships are significant differs amongst seasons and suggests that different circulatory features are more or less important in different seasons.
4. The rainfall/moisture convergence relationship is a large-scale feature of the basin; it does not occur at all subdomains in all seasons.
5. Model rainfall depends on water vapor transport into the basin across different boundaries and at different heights. A targeted measurement campaign at certain boundaries could help to constrain the spectrum of model rainfall.
6. Model simulations of the large-scale circulation play a significant role in differentiating between model rainfall. Model sea surface temperature biases and topography schemes are possible controls on this relationship; these will be addressed in future work.

The Congo Basin remains a significant challenge for climate modeling due to the dearth of observational data and the unlikelihood of making significant gains in observation in the coming years. Nevertheless, there is scope for a much deeper understanding of the dynamics of individual climate models, and this study comprises a first assessment of the differences between model climatologies for this region. Process-based model evaluation techniques are increasingly being used to understand why models behave as they do and whether models can be grouped or ranked by their characteristics. This study also highlights the dangers of using model ensembles as a “best guess” for current or future climate scenarios in regions with poor observational coverage. For central Africa, the use of the ensemble mean is misleading and is likely to mask important climate information. Crucially, this paper has outlined the potential utility of processes such as moisture flux convergence in constraining parameterized outputs, in the absence of high-resolution model data sets which are needed to capture tropical convection processes explicitly. In addition, it highlights the potential utility of long-term field campaigns on the boundaries of the Congo Basin, which fall outside both the physical and practical barriers to access, and may provide important insights into local/regional/global interactions.

A logical next step is to assess the regional circulation for drivers which may be common amongst models or particular subgroups of models. Indian and Atlantic Ocean SST biases are likely to play a role in setting up the moisture dynamics which feed into the basin. The role of convection/convergence feedbacks must also be assessed with respect to the overturning circulation. Topography, and relatedly model resolution, has also emerged as a local factor which may be of significance in particular seasons. Despite the enormity of the challenges still facing Congo climate science, these approaches appear fruitful and provide a possible mechanism for confronting the wide array of future climate trajectories produced by models. This step is vital for providing credible climate products for decision-makers in this region.

Acknowledgments

The GCM data used in this study were made available through the Earth System Grid Federation (ESGF) Peer-to-Peer system (<https://pcmdi.llnl.gov/search/cmip5/>). We also acknowledge NOAA/OAR/ESRL PSD and ECMWF for making available the NCEP and ERA-I data sets. The first author is fully funded by the National Environmental Research Council via a Doctoral Training Programme (grant NE/L002612/1). Richard Washington is partly supported by the NERC-funded IMPALA (NE/M017206/1) and UMFULA (NE/M020207/1) programs. The authors acknowledge the helpful inputs of Sebastian Engelstaedter, Neil Hart, and Callum Munday.

References

- Adler, R. F., *et al.* (2003), The Version-2 Global Precipitation Climatology Project (GPCP) monthly precipitation analysis (1979–present), *J. Hydrometeorol.*, 4(6), 1147–1167, doi:10.1175/1525-7541(2003)004<1147:TVGPCP>2.0.CO;2.
- Aguilar, E., *et al.* (2009), Changes in temperature and precipitation extremes in western central Africa, Guinea Conakry, and Zimbabwe, 1955–2006, *J. Geophys. Res.*, 114, D02115, doi:10.1029/2008JD011010.
- Aloysius, N. R., J. Sheffield, and E. F. Wood (2016), Evaluation of historical and future simulations of precipitation and temperature in central Africa from CMIP5 climate models, *J. Geophys. Res. Atmos.*, 121, 130–152, doi:10.1002/2015JD023656.
- Baccini, A., *et al.* (2012), Estimated carbon dioxide emissions from tropical deforestation improved by carbon-density maps, *Nat. Clim. Change*, 2(3), 182–185, doi:10.1038/nclimate1354.

- Bentsen, M., et al. (2013), The Norwegian Earth system model, NorESM1-M—Part 1: Description and basic evaluation of the physical climate, *Geosci. Model Dev. Discuss.*, 6, 687–720, doi:10.5194/gmd-6-687-2013.
- Burde, G. I., A. Zangvil, and P. J. Lamb (1996), Estimating the role of local evaporation in precipitation for a two-dimensional region, *J. Clim.*, 9(6), 1328–1338, doi:10.1175/1520-0442(1996)009<1328:ETROLE>2.0.CO;2.
- Camberlin, P., S. Janicot, and I. Poccarr (2001), Seasonality and atmospheric dynamics of the teleconnection between African rainfall and tropical ocean surface temperatures, *Int. J. Climatol.*, 21, 973–1005.
- Chou, C., J. D. Neelin, J. Y. Tu, and C. T. Chen (2006), Regional tropical precipitation change mechanisms in ECHAM4/OPYC3 under global warming, *J. Clim.*, 19(17), 4207–4223, doi:10.1175/JCLI3858.1.
- Christensen, J. H., et al. (2013), Climate phenomena and their relevance for future regional climate change, in *Climate Change 2013: The Physical Science Basis. Contribution of Working Group I to the Fifth Assessment Report of the Intergovernmental Panel on Climate Change*, edited by T. F. Stocker et al., pp. 1217–1308, Cambridge Univ. Press, Cambridge, U. K., and New York.
- Collier, M., and P. Uhe (2012), CMIP5 datasets from the ACCESS1.0 and ACCESS1.3 coupled climate models, CAWCR Tech. Rep. No. 059, Centre for Australian Weather and Climate Research, ISBN:20978-1-922173-29-4.
- Collins, M., et al. (2013), Long-term climate change: Projections, commitments and irreversibility, in *Climate Change 2013: The Physical Science Basis. Working Group I Contribution to the IPCC Fifth Assessment Report*, edited by T. F. Stocker et al., pp. 1029–1136, Cambridge Univ. Press, Cambridge, U. K., and New York.
- Cook, K. H., and E. K. Vizy (2006), Coupled model simulations of the West African monsoon system: Twentieth- and twenty-first-century simulations, *J. Clim.*, 19(15), 3681–3703, doi:10.1175/JCLI3814.1.
- Cook, K. H., and E. K. Vizy (2015), The Congo Basin Walker circulation: Dynamics and connections to precipitation, *Clim. Dyn.*, doi:10.1007/s00382-015-2864-y.
- Davey, M., et al. (2002), STOIC: A study of coupled model climatology and variability in tropical ocean regions, *Clim. Dyn.*, 18(5), 403–420, doi:10.1007/s00382-001-0188-6.
- Dee, D. P., et al. (2011), The ERA-Interim reanalysis: Configuration and performance of the data assimilation system, *Q. J. R. Meteorol. Soc.*, 137(656), 553–597, doi:10.1002/qj.828.
- Dezfuli, A. K., and S. E. Nicholson (2011), A note on long-term variations of the African easterly jet, *Int. J. Climatol.*, 31(13), 2049–2054, doi:10.1002/joc.2209.
- Dieppois, B., M. Rouault, and M. New (2015), The impact of ENSO on Southern African rainfall in CMIP5 ocean atmosphere coupled climate models, *Clim. Dyn.*, 45(9–10), 2425–2442, doi:10.1007/s00382-015-2480-x.
- Donner, L. J., et al. (2011), The dynamical core, physical parameterizations, and basic simulation characteristics of the atmospheric component AM3 of the GFDL global coupled model CM3, *J. Clim.*, 24(13), 3484–3519, doi:10.1175/2011JCLI3955.1.
- Dufresne, J. L., et al. (2013), Climate change projections using the IPSL-CM5 Earth System Model: From CMIP3 to CMIP5, *Clim. Dyn.*, 40(9–10), 2123–2165, doi:10.1007/s00382-012-1636-1.
- Dunne, J. P., et al. (2013), GFDL's ESM2 global coupled climate-carbon Earth system models. Part II: Carbon system formulation and baseline simulation characteristics, *J. Clim.*, 26(7), 2247–2267, doi:10.1175/JCLI-D-12-00150.1.
- Flato, G., et al. (2013), Evaluation of climate models, in *Climate Change 2013: The Physical Science Basis. Contribution of Working Group I to the Fifth Assessment Report of the Intergovernmental Panel on Climate Change*, edited by T. F. Stocker et al., pp. 741–866, Cambridge Univ. Press, Cambridge, U. K., and New York.
- Gulizia, C., and I. Camilloni (2014), Comparative analysis of the ability of a set of CMIP3 and CMIP5 global climate models to represent precipitation in South America, *Int. J. Climatol.*, 35(4), 583–595, doi:10.1002/joc.4005.
- Haensler, A., D. Jacob, P. Kabat, and F. Ludwig (2013), Assessment of projected climate change signals over central Africa based on a multitude of global and regional climate projections, *Climate Change Scenarios for the Congo Basin*, Climate Service Center Report 11.
- Hagedorn, R., F. J. Doblas-Reyes, and T. N. Palmer (2005), The rationale behind the success of multimodel ensembles in seasonal forecasting—I. Basic concept, *Tellus A Dyn. Meteorol. Oceanogr.*, 57(3), 219–233, doi:10.1111/j.1600-0870.2005.00103.x.
- Hansingo, K., and C. J. C. Reason (2009), Modelling the atmospheric response over Southern Africa to SST forcing in the southeast tropical Atlantic and southwest subtropical Indian Oceans, *Int. J. Climatol.*, 29, 1001–1012, doi:10.1002/joc.
- Harris, I., P. D. Jones, T. J. Osborn, and D. H. Lister (2014), Updated high-resolution grids of monthly climatic observations—The CRU TS3.10 Dataset, *Int. J. Climatol.*, 34(3), 623–642, doi:10.1002/joc.3711.
- Held, I., and B. Soden (2006), Robust responses of the hydrological cycle to global warming, *J. Clim.*, 19(21), 5686–5699, doi:10.1175/JCLI3990.1.
- Hirst, A. C., and S. Hastenrath (1983), Atmosphere-ocean mechanisms of climate anomalies in the Angola-tropical Atlantic sector, *J. Phys. Oceanogr.*, 13, 1146–1157.
- Huffman, G. J., D. T. Bolvin, E. J. Nelkin, D. B. Wolff, R. F. Adler, G. Gu, Y. Hong, K. P. Bowman, and E. F. Stocker (2007), The TRMM Multisatellite Precipitation Analysis (TMPA): Quasi-global, multiyear, combined-sensor precipitation estimates at fine scales, *J. Hydrometeorol.*, 8(1), 38–55, doi:10.1175/JHM560.1.
- Jackson, B., S. E. Nicholson, and D. Klotter (2009), Mesoscale convective systems over western equatorial Africa and their relationship to large-scale circulation, *Mon. Weather Rev.*, 137(4), 1272–1294, doi:10.1175/2008MWR2525.1.
- James, R., and R. Washington (2013), Changes in African temperature and precipitation associated with degrees of global warming, *Clim. Change*, 117(4), 859–872, doi:10.1007/s10584-012-0581-7.
- James, R., R. Washington, and R. Jones (2015), Process-based assessment of an ensemble of climate projections for West Africa, *J. Geophys. Res. Atmos.*, 120, 1221–1238, doi:10.1002/2014JD022513.
- Jeffrey, S. J., L. D. Rotstayn, M. A. Collier, S. M. Dravitzki, C. Hamalainen, C. Moeseneder, K. K. Wong, and J. I. Syktus (2013), Australia's CMIP5 submission using the CSIRO Mk3.6 model, *Aust. Meteorol. Oceanogr. J.*, 63, 1–13.
- Ji, D., et al. (2014), Description and basic evaluation of Beijing Normal University Earth System Model (BNU-ESM) version 1, *Geosci. Model Dev.*, 7(5), 2039–2064, doi:10.5194/gmd-7-2039-2014.
- Jones, C. D., et al. (2011), The HadGEM2-ES implementation of CMIP5 centennial simulations, *Geosci. Model Dev.*, 4(3), 543–570.
- Kalnay, E., et al. (1996), The NCEP/NCAR 40-year reanalysis project, *Bull. Am. Meteorol. Soc.*, 77(3), 437–471, doi:10.1175/1520-0477(1996)077<0437:TNYRP>2.0.CO;2.
- Kay, G., and R. Washington (2008), Future Southern African summer rainfall variability related to a southwest Indian Ocean dipole in HadCM3, *Geophys. Res. Lett.*, 35, L12701, doi:10.1029/2008GL034180.
- Lau, K. M., S. S. P. Shen, K.-M. Kim, and H. Wang (2006), A multimodel study of the twentieth-century simulations of Sahel drought from the 1970s to 1990s, *J. Geophys. Res.*, 111, D07111, doi:10.1029/2005JD006281.

- Maidment, R. I., D. Grimes, R. P. Allan, E. Tarnavsky, M. Stringer, T. Hewison, R. Roebeling, and E. Black (2014), The 30 year TAMSAT African Rainfall Climatology And Time series (TARCAT) data set, *J. Geophys. Res. Atmos.*, *119*, 10,619–10,644, doi:10.1002/2014JD021927.
- Malhi, Y., et al. (2013), African rainforests: Past, present and future, *Philos. Trans. R. Soc. London B Biol. Sci.*, *368*(1625), doi:10.1098/rstb.2012.0312.
- Marsland, S. J., H. Haak, J. H. Jungclaus, M. Latif, and F. Roske (2003), The Max-Planck-Institute global ocean/sea ice model with orthogonal curvilinear coordinates, *Ocean Model.*, *5*(2), 91–127, doi:10.1016/S1463-5003(02)00015-X.
- McCollum, J. R., A. Gruber, and M. B. Ba (2000), Discrepancy between gauges and satellite estimates of rainfall in equatorial Africa, *J. Appl. Meteorol.*, *39*(5), 666–679, doi:10.1175/1520-0450-39.5.666.
- Moufouma-Okia, W., and R. Jones (2014), Resolution dependence in simulating the African hydroclimate with the HadGEM3-RA regional climate model, *Clim. Dyn.*, *44*(3–4), 609–632, doi:10.1007/s00382-014-2322-2.
- Neale, R. B., et al. (2012), Description of the NCAR Community Atmosphere Model (CAM 5.0), NCAR Tech. Notes, National Center for Atmospheric Research.
- Neelin, J. D., M. Munnich, H. Su, J. E. Meyerson, and C. E. Holloway (2006), Tropical drying trends in global warming models and observations, *Proc. Natl. Acad. Sci. U.S.A.*, *103*, 6110–6115, doi:10.1073/pnas.0601798103.
- Nicholson, S. E., and A. K. Dezfuli (2013), The relationship of rainfall variability in western equatorial Africa to the tropical oceans and atmospheric circulation. Part I: The boreal spring, *J. Clim.*, *26*(1), 45–65, doi:10.1175/JCLI-D-11-00653.1.
- Nicholson, S. E., and D. Entekhabi (1987), Rainfall variability in equatorial and Southern Africa: Relationships with sea surface temperatures along the southwestern coast of Africa, *J. Clim. Appl. Meteorol.*, *26*(5), 561–578, doi:10.1175/1520-0450(1987)026<0561:RVIEAS>2.0.CO;2.
- Nicholson, S. E., and J. P. Grist (2003), The seasonal evolution of the atmospheric circulation over West Africa and equatorial Africa, *J. Clim.*, *16*(7), 1013–1030, doi:10.1175/1520-0442(2003)016<1013:TSEOTA>2.0.CO;2.
- Nicholson, S. E., et al. (2003), Validation of TRMM and other rainfall estimates with a high-density gauge dataset for West Africa. Part II: Validation of TRMM rainfall products, *J. Appl. Meteorol.*, *42*(10), 1355–1368, doi:10.1175/1520-0450(2003)042<1355:VOTAOR>2.0.CO;2.
- Nicholson, S. E., A. K. Dezfuli, and D. Klotter (2012), A two-century precipitation dataset for the continent of Africa, *Bull. Am. Meteorol. Soc.*, *93*(8), 1219–1231, doi:10.1175/BAMS-D-11-00212.1.
- Palmer, T. N., F. J. Doblas-Reyes, R. Hagedorn, and A. Weisheimer (2005), Probabilistic prediction of climate using multi-model ensembles: From basics to applications, *Philos. Trans. R. Soc. B*, *360*(1463), 1991–1998, doi:10.1098/rstb.2005.1750.
- Pokam, W. M., L. A. Tchotchou Djotang, and F. K. Mkankam (2012), Atmospheric water vapor transport and recycling in equatorial central Africa through NCEP/NCAR reanalysis data, *Clim. Dyn.*, *38*(9), 1715–1729, doi:10.1007/s00382-011-1242-7.
- Pokam, W., C. L. Bain, R. S. Chadwick, R. Graham, D. J. Sonwa, and F. M. Kamga (2014), Identification of processes driving low-level westerlies in west equatorial Africa, *J. Clim.*, *27*(11), 4245–4262, doi:10.1175/JCLI-D-13-00490.1.
- Reichler, T., and J. Kim (2008), How well do coupled models simulate today's climate?, *Bull. Am. Meteorol. Soc.*, *89*(3), 303–311, doi:10.1175/BAMS-89-3-303.
- Richter, I., and S. P. Xie (2008), On the origin of equatorial Atlantic biases in coupled general circulation models, *Clim. Dyn.*, *31*(5), 587–598, doi:10.1007/s00382-008-0364-z.
- Richter, I., S. P. Xie, A. T. Wittenberg, and Y. Masumoto (2012), Tropical Atlantic biases and their relation to surface wind stress and terrestrial precipitation, *Clim. Dyn.*, *38*(5–6), 985–1001, doi:10.1007/s00382-011-1038-9.
- Rowell, D. P., C. A. Senior, M. Vellinga, and R. J. Graham (2015), Can climate projection uncertainty be constrained over Africa using metrics of contemporary performance?, *Clim. Change*, *134*(4), 621–633, doi:10.1007/s10584-015-1554-4.
- Samba, G., and D. Nganga (2012), Rainfall variability in Congo-Brazzaville: 1932–2007, *Int. J. Climatol.*, *32*(6), 854–873, doi:10.1002/joc.2311.
- Sandjon, A. T., A. Nzeukou, and C. Tchawoua (2012), Intraseasonal atmospheric variability and its interannual modulation in central Africa, *Meteorol. Atmos. Phys.*, *117*, 167–179.
- Schmidt, G. A., et al. (2013), Configuration and assessment of the GISS ModelE2 contributions to the CMIP5 archive, *J. Adv. Model. Earth Syst.*, *6*(1), 141–184, doi:10.1002/2013MS000265.
- Schneider, U., A. Becker, P. Finger, A. Meyer-Christoffer, B. Rudolf, and M. Ziese (2015), GPCC full data reanalysis version 7.0 at 0.5: Monthly land-surface precipitation from rain-gauges built on GTS-based and historic data, doi:10.5676/DWD_GPCC/FD_M_V7_050.
- Scoccimarro, E., S. Gualdi, A. Bellucci, A. Sanna, P. G. Fogli, E. Manzini, M. Vichi, P. Oddo, and A. Navarra (2011), Effects of tropical cyclones on ocean heat transport in a high-resolution coupled general circulation model, *J. Clim.*, *24*(16), 4368–4384, doi:10.1175/2011JCLI4104.1.
- Taylor, K. E., R. J. Stouffer, and G. A. Meehl (2012), An overview of CMIP5 and the experiment design, *Bull. Am. Meteorol. Soc.*, *93*(4), 495–498, doi:10.1175/BAMS-D-11-00094.1.
- Tebaldi, C., and R. Knutti (2007), The use of the multi-model ensemble in probabilistic climate projections, *Philos. Trans. A. Math. Phys. Eng. Sci.*, *365*(1857), 2053–2075, doi:10.1098/rsta.2007.2076.
- Titchner, H. A., and N. A. Rayner (2014), The Met Office Hadley Centre sea ice and sea surface temperature data set, version 2: 1. Sea ice concentrations, *J. Geophys. Res. Atmos.*, *119*, 2864–2889, doi:10.1002/2013JD020316.
- Todd, M. C., and R. Washington (2004), Climate variability in central equatorial Africa: Influence from the Atlantic sector, *Geophys. Res. Lett.*, *31*, L23202, doi:10.1029/2004GL020975.
- Volodro, A., et al. (2011), The CNRM-CM5.1 global climate model: Description and basic evaluation, *Clim. Dyn.*, *40*(9), 2091–2121, doi:10.1007/s00382-011-1259-y.
- Wahl, S., M. Latif, W. Park, and N. Keenlyside (2009), On the tropical Atlantic SST warm bias in the Kiel climate model, *Clim. Dyn.*, *36*(5–6), 891–906, doi:10.1007/s00382-009-0690-9.
- Wang, C., L. Zhang, S.-K. Lee, L. Wu, and C. R. Mechoso (2014), A global perspective on CMIP5 climate model biases, *Nat. Clim. Change*, *4*(3), 201–205.
- Washington, R., M. Harrison, D. Conway, E. Black, A. Challinor, D. Grimes, R. Jones, A. Morse, G. Kay, and M. Todd (2006), African climate change: Taking the shorter route, *Bull. Am. Meteorol. Soc.*, *87*(10), 1355–1366, doi:10.1175/BAMS-87-10-1355.
- Washington, R., R. James, H. Pearce, W. M. Pokam, and W. Moufouma-Okia (2013), Congo Basin rainfall climatology: Can we believe the climate models?, *Philos. Trans. R. Soc. Lond. B Biol. Sci.*, *368*(1625), 20120296, doi:10.1098/rstb.2012.0296.
- Watanabe, M., et al. (2010), Improved climate simulation by MIROC5: Mean states, variability, and climate sensitivity, *J. Clim.*, *23*(23), 6312–6335, doi:10.1175/2010JCLI3679.1.
- Watanabe, S., et al. (2011), MIROC-ESM: Model description and basic results of CMIP5-20c3m experiments, *Geosci. Model Dev. Discuss.*, *4*(2), 1063–1128, doi:10.5194/gmdd-4-1063-2011.
- Webster, P. J. (1983), Large-scale structure of the tropical atmosphere, in *Large Scale Dynamical Processes in the Atmosphere*, edited by B. Hoskins and R. Pearce, pp. 235–275, Academic Press, New York.

- Williams, C. A., N. P. Hanan, J. C. Neff, R. J. Scholes, J. A. Berry, A. S. Denning, and D. F. Baker (2007), Africa and the global carbon cycle, *Carbon Balance Manage*, 13(3), doi:10.1186/1750-0680-2-3.
- Xie, P., and P. A. Arkin (1997), Global precipitation: A 17-year monthly analysis based on gauge observations, satellite estimates, and numerical model outputs, *Bull. Am. Meteorol. Soc.*, 78(11), 2539–2558, doi:10.1175/1520-0477(1997)078<2539:GPAYMA>2.0.CO;2.
- Xie, P., J. E. Janowiak, P. A. Arkin, R. Adler, A. Gruber, R. Ferraro, G. J. Huffman, and S. Curtis (2003), GPCP pentad precipitation analyses: An experimental dataset based on gauge observations and satellite estimates, *J. Clim.*, 16(13), 2197–2214, doi:10.1175/2769.1.
- Xu, Z., P. Chang, I. Richter, W. Kim, and G. Tang (2014), Diagnosing southeast tropical Atlantic SST and ocean circulation biases in the CMIP5 ensemble, *Clim. Dyn.*, 43, 3123–3145, doi:10.1007/s00382-014-2247-9.
- Yang, D., and O. A. Saenko (2012), Ocean heat transport and its projected change in CanESM2, *J. Clim.*, 25(23), 8148–8163, doi:10.1175/JCLI-D-11-00715.1.
- Yin, L., R. Fu, E. Shevliakova, and R. E. Dickinson (2013), How well can CMIP5 simulate precipitation and its controlling processes over tropical South America?, *Clim. Dyn.*, 41(11–12), 3127–3143, doi:10.1007/s00382-012-1582-y.
- Yukimoto, S., et al. (2011), Meteorological Research Institute-Earth System Model Version 1 (MRI-ESM1), Technical Reports No. 64.